AN ABSTRACT OF THE THESIS OF

Orhan Can Özdural for the degree of Doctor of Philosophy in
Electrical and Computer Engineering presented on February 21, 2007.

Title: Performance-Improving Techniques for Wireless Systems

Abstract approved: ______________________________

Huaping Liu

In this thesis, maximum likelihood Doppler frequency estimation and phase noise suppression algorithms for Orthogonal Frequency Division Multiplexing (OFDM) systems are presented. A novel handover decision algorithm for wireless systems, called predictive base station switching (PBSS), is also introduced.

The maximum Doppler Frequency is the ratio of the speed of the mobile user and the carrier frequency. The Doppler frequency information of each mobile can be exploited to minimize the number of handover scenarios and to improve channel estimation. The estimation of this quantity in time-varying multipath channels is performed in this thesis by a frequency-domain approach that utilizes pilot subcarriers, which are commonly implemented in most practical OFDM systems. In the proposed estimator, the effect of the intercarrier interference (ICI) caused by the time-varying fading is taken into consideration with a proper model for accurate results. The Cramer-Rao bounds are also derived and simulation results are provided to quantify the performance of the algorithm.

This thesis also presents a maximum likelihood approach exploiting the OFDM pilot subcarriers to suppress phase noise due to imperfect local oscillators. This algorithm does not require perfect channel equalization and is applicable for

the two common types of oscillators: phase-locked and free-running oscillators. Furthermore, doubly-selective fading is considered rather than assuming time-invariant and/or flat fading channels.

Finally, a new handover decision algorithm, PBSS, is presented. PBSS is designed for broadband wireless access (BWA) systems (where users can travel at vehicular speeds) that typically have small cell sizes due to high-data-rate transmission. High-mobility users of BWA systems usually need to perform frequent handovers, which degrades the overall network performance. PBSS uses mobile speed and direction information to reduce the number of handovers without degrading the received signal level. Simulation results show that PBSS performs better than algorithms solely based on information of signal strength and distance and has a comparable outage probability, even when the users move randomly or accurate direction and speed information is unavailable.

Performance-Improving Techniques for Wireless Systems

by

Orhan Can Özdural

A THESIS

submitted to

Oregon State University

in partial fulfillment of
the requirements for the
degree of

Doctor of Philosophy

Presented February 21, 2007
Commencement June 2007

Doctor of Philosophy thesis of Orhan Can Özdural presented on February 21, 2007

APPROVED:

Major Professor, representing Electrical and Computer Engineering

---

Director of the School of Electrical Engineering and Computer Science

---

Dean of the Graduate School

I understand that my thesis will become part of the permanent collection of Oregon State University libraries. My signature below authorizes release of my thesis to any reader upon request.

Orhan Can Özdural, Author

ACKNOWLEDGMENTS

I would like to express my genuine gratitude to my supervisor Dr. Huaping Liu for the support he provided me through my graduate studies. Without his positive, honest and friendly attitude; his great technical insight and guidance, this thesis could not have been completed. I consider myself extremely lucky to have him as a mentor.

I also would like to thank my committee members, Dr. Mario E. Magaña, Dr. Larry Marple, Dr. Zhongfeng Wang, Dr. Luca Lucchese and Dr. Larry Chen for their continuous support and constructive comments on my research. I am also grateful to my supervisors at Intel Corporation, Dr. Ali Sadri, Dr. Sasan H. Ardalan and Dr. Yang-Seok Choi for allowing me to improve my knowledge in the field and to observe how theory applies to real-life products. I am further thankful to Dr. Yang-Seok Choi for the collaborative work on maximum Doppler Frequency Estimation. I also would like to thank to past and current members of our group, especially Jie Gao, Liang Xian, Shiwei Zhao, Ferhat Yildirim and Weiting Chen.

Finally, I would like to thank my parents. Clearly, without their endless support and encouragement, I would not be where I am now.

TABLE OF CONTENTS

Page

TABLE OF CONTENTS (Continued)

Page

LIST OF FIGURES

Figure Page

Figure Page

LIST OF TABLES

DEDICATION

I dedicate this thesis to my grandmother Nermin Özdural.

Performance-Improving Techniques for Wireless Systems

1. INTRODUCTION

1.1. Background and Motivation

It is not a dream anymore to have a hand-held device that not only merges mobile phone and personal digital assistant (PDA) devices together, but also performs as MP3 player and an access point to a certain network. Such devices must effectively combine different wireless standards. Such a device would need the capability of connecting to *Wireless Local Area Networks*, *Personal Area Networks* and *Wide-Area Networks*. Thus improving the performance of each of these wireless standards would be a very significant contribution to the ongoing research efforts in the area.

As wireless systems are used by more people and become a permanent part of our daily lives, future wireless systems in all forms will have to provide improved data rates for a given bandwidth to address the needs of new applications, standards and devices. To be able to provide more bandwidth, the performance of the wireless systems must be optimized. In this thesis, three novel techniques to improve the performance of Wireless Systems are provided, each focusing on a different aspect of the problem.

TABLE 1.1. Comparison of different Wi-Fi standards.

Standard	**Modulation Type**	**Max. Data Rate**	**Op. Frequency**
802.11b	CCK/DSSS	11Mbps	2.4GHz
802.11g	OFDM	54Mbps	2.4GHz
802.11a	OFDM	54Mbps	5GHz
802.11n	MIMO/OFDM	200Mbps	2.4 or 5GHz

1.1.1. Comparison of Different Wireless Standards

1.1.1.1. Wireless Local Area Networks (WLAN)

Wireless Local Area Networks (WLAN) can be considered as an implementation of Local Area Networks (LAN) using microcellular wireless systems, which cover a small geographic area, like a home, an office or a small-sized building. The smaller geographic range allows WLAN to have higher data rates compared to larger wireless networks. These networks are also frequently called Wi-Fi networks, which is a trademark of the Wi-Fi alliance. This alliance is a trade organization that also certifies equipment compliance with IEEE 802.11 standards [1]. The variations between different IEEE 802.11 schemes are presented in the Table 1.1.

The first Wi-Fi standard, 802.11b was based on a form of Direct-Sequence Spectrum Spread (DSSS) CDMA modulation scheme called Complementary Code Keying (CCK) and operates at 2.4GHz. The following standard, 802.11g, has changed the modulation scheme to OFDM with backwards compatibility with 802.11b schemes. Later, due to the relatively high interference at 2.4GHz, a new standard called 802.11a, also based on OFDM, has been developed operating at

5GHz. The next addition to the 802.11 standards will be 802.11n, which will have a Multiple-Input Multiple Output (i.e. using multiple antennas at both the transmitter and the receiver side) OFDM (MIMO-OFDM) scheme, which will considerably increase the data rate due to the increase in the capacity provided by spatial multiplexing [2], [3].

WLAN systems allow LANs to be deployed without any cables, which reduces the cost of network deployment. Another important advantage WLAN brings over conventional LAN is the ease of network expansion, making it possible to connect new devices to the same network. Unlike cellular carriers and other cable-based broadband Internet access schemes, Wi-Fi is based on a set of global standards, which allow the devices to work in any country independent of the country of origin of the device. The wide-availability of public hot-spots is also another advantage of WLAN systems, which is caused by the relatively low silicon pricing of such systems.

However, WLAN systems also have some disadvantages associated with them, their small geographic area being the foremost one. Furthermore, the spectrum assignments vary in different regions of the world, which requires the current region to be determined during the initial network setup. Another problem arises if the number of users of a WLAN system is high, increasing inter-channel interference. The bands in which IEEE 802.11 standards operate is the unlicensed spectrum near 2.4GHz (except for 802.11a, which operates around 5GHz), and many other wireless devices, including amateur radio, using this range might cause significant disturbance.

The information security problems of WLAN systems further compound the problem, as the information provided by the user might be intercepted. The regular encryption standard, Wired Equivalent Privacy (WEP), has been shown to be breakable even when correctly configured [4]. Secondary encryption standards known as Wi-Fi Protected Access (WAP and WAP2), offer stronger encryption schemes if appropriate passwords are used. However, the standard mode of operation of public WLAN access points is generally encryption-free, as it would not make sense to encrypt the information if the password would be available to everyone.

1.1.1.2. Personal Area Networks (PAN)

Personal Area Networks (PAN) are intended to connect two devices that are close to each other. The most common examples of PAN networks are Bluetooth [5] or Wireless USB [6]. These networks are called *personal* as the devices they connect theoretically belong to the same person: peripherals such as keyboard, mouse, printer, digital camera to a computer; computer, palm or mobile phone to a headset; mobile phone to PAN equipped vehicle; game controller to the games console; a laptop computer to a desktop station, etc. The devices can even be in different rooms, as long as the signal level is above a certain level. The reach of PAN is generally limited to a few meters.

The inherent difference between WLAN and PAN lies in their design goals. Some PAN types (such as Bluetooth) use the same spectrum as WLAN. WLAN devices are built to fully replace cable-based LANs, whereas PANs are intended to provide a wireless low-power, high-efficiency scheme to allow basic communication between different devices and their peripherals. WLAN has a higher power consumption, larger geographical range, higher data rates and better security. However, it would be truly unwise to expect a headset to connect to a mobile phone via WLAN, due to size, cost and power consumption considerations. This is the reason why, many devices are equipped with both standards.

1.1.1.3. Wide-Area Networks (WAN)

Wide-Area Networks (WAN) can be classified as high data rate networks that cover larger areas compared to WLAN. The range of WAN systems depend on the coverage of the service provider, however it would be reasonable to assume they will be available in all major city centers in the near future.

To provide examples of WAN systems, one can cite schemes that work over existing 2G cellular systems, such as General Packet Radio Service (GPRS) and Enhanced Data rates for GSM Evolution (EDGE); pure 3G systems such as Evolution-Data Optimized (EV-DO) for CDMA2000 standard, High-Speed Uplink Packet Access (HSUPA) and High-Speed Downlink Packet Access (HSDPA) for Universal Mobile Telecommunications System (UMTS) standard; and broadband wireless access schemes, such as (Worldwide Interoperability for Microwave Access) WIMAX (i.e. IEEE 802.16 standard).

It should be noted that 2G extension schemes, such as GPRS, are developed strictly for mobile phone applications, whereas 3G schemes, such as EV-DO, can be considered as a means for broadband Internet access replacement. WIMAX, which is purely packet-switched, is developed independent of a cellular network and can provide higher bandwidths. Generally all 2.5G/3G systems can actually be considered as add-ons to what is essentially a voice service. WIMAX, theoretically, can also provide voice services through Voice-over-IP (VoIP). WIMAX is also considered as a Metropolitan Area Network (MAN).

TABLE 1.2. Comparison of WLAN and WAN systems.

Standard	**Type**	**Uplink**	**Downlink**	**Indoor Range**
WI-FI / 802.11b	WLAN	11Mbps	11Mbps	∼30m
WI-FI / 802.11g	WLAN	54Mbps	54Mbps	∼30m
WI-FI / 802.11a	WLAN	54Mbps	54Mbps	∼30m
WI-FI / 802.11n	WLAN	200Mbps	200Mbps	∼50m
GPRS	WAN	0.080Mbps	0.040Mbps	
EDGE	WAN	0.474Mbps	0.474Mbps	
EV-DO 1x Rev. B	WAN	4.9Mbps	1.8Mbps	
HSDPA	WAN	14.4Mbps	0.384Mbps	
HSUPA	WAN	14.4Mbps	5.760Mbps	
WIMAX / 802.16e	WAN	70Mbps	70Mbps	

It is important to note however, that the use and design considerations of WLAN and WAN (especially WIMAX) systems are completely different, as it was the case for PAN and WLAN systems. WAN systems basically have a higher geographical coverage, and this allows continuous network access regardless of the location of the user in a WAN deployed urban area, however the data rate might be relatively low. WIMAX, on the other hand, is further intended to replace Digital Subscriber Line (DSL) for Business Offices.

Table 1.2 provides the comparison of different WLAN and WAN systems in terms of downlink/uplink capacity, type of wireless service and the indoor range of the service (if applicable) [7].

In any case, it would not be unreasonable to expect a hand-held device to be compatible with at least one PAN (e.g. Bluetooth), one WLAN (e.g. IEEE

802.11n) and one WAN (e.g. EV-DO) standard along with a voice service. Thus, helping to solve the problems of these different but necessary technologies, as done in this thesis, would be a very important contribution to the ongoing research and development efforts on wireless systems.

1.1.2. Maximum Likelihood (ML) Maximum Doppler Frequency Estimation

Orthogonal frequency division multiplexing (OFDM) has been adopted by many Wi-Fi and WAN wireless standards such as IEEE 802.11a [9] and 802.16e [10] and has been implemented in many practical systems. OFDM systems are chosen over other alternatives as they have superior performance in frequency-selective channels, and they allow the efficient use of the available bandwidth.

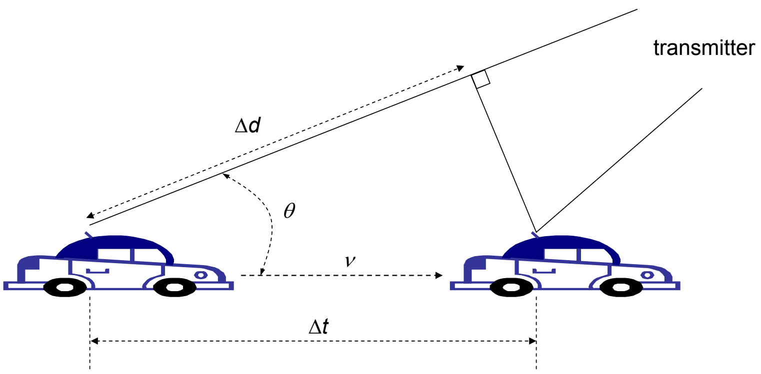

FIGURE 1.1. Geometry associated with Doppler shift.

To be able to explain the effect of Doppler, one can make use of Fig. 1.1 [8]. In this figure, the received signal may undergo a narrowband Doppler shift of $f_D = v\ cos\theta/\lambda$, where θ is considered to be the arrival angle of the received signal relative to the direction of motion, v is the receiver velocity towards or away from the transmitter in the direction of motion, and $\lambda = c/f_c$ is the signal wavelength ($c = 3\times10^8$ m/s is the speed of light, and f_c is the carrier frequency). The Doppler shift basically is the result of transmitter or receiver movement over a short time interval Δt, which causes a slight change in the distance (Δd) the transmitted signal needs to travel to reach the receiver ($\Delta d = v\Delta t\cos\theta$). The phase change due to this path length difference is $\Delta\phi = 2\pi v\Delta t\cos\theta/\lambda$. The Doppler frequency can then be obtained as in Eq. 1.1 [8]

$$f_D = \frac{1}{2\pi}\frac{\Delta\phi}{\Delta t} = \cos\theta\ v/\lambda. \tag{1.1}$$

The maximum Doppler frequency, f_d, can then be obtained as the maximum f_D, which is the ratio of the speed of the mobile user and the wavelength of the carrier, $f_d = v/\lambda$. Knowledge of mobile speeds is critical in improving the performance of multi-cell wireless communication systems. For example, in the pico-cell deployment overlaying with existing macro-cells, the Doppler frequency information of each mobile allows optimization of user assignments to proper base stations, and thus minimizes the number of handover scenarios. The mobile speed information is also very critical for implementing a number of physical- and network-layer functions such as adaptive and fast link adaptation, and accurate channel prediction. Thus, the scheduler gain due to multiuser diversity and spectral efficiency of the system can be increased.

In [18], an autocorrelation-based scheme for maximum-Doppler-frequency estimation was proposed for single-carrier systems, where the estimate is obtained using the envelope of the received signal. In [19], a method based on the differentials of the channel estimates is employed for the estimation process. Another method based on the level-crossing rates was proposed in [20]. In most OFDM systems, a cyclic prefix (CP), which is the replica of the OFDM symbol tail, is used as the guard interval. In [21], the correlation between the tail of the OFDM symbol and the guard interval was exploited to estimate f_d, where the effects of intersymbol interference (ISI) was not considered. In [22], the estimate of f_d is obtained via a maximum-likelihood (ML) based time-domain method for TDMA and CDMA systems. The application of this algorithm to OFDM systems was presented in [23], where time-domain channel estimates were used to obtain the maximum Doppler frequency estimates. In this model, the channel is not estimated based on pilot subcarriers, but by using preambles and inserting frequent mid-ambles, and in the frequency domain approach, the ICI is ignored. Thus, an error floor is observed.

In this thesis, an ML algorithm of Doppler frequency estimation for OFDM systems is presented in Chapter 3. This part of the thesis focuses on wireless systems (generally WAN or WLAN) that employ the OFDM scheme.

1.1.3. ML Phase Noise Suppression

Although OFDM systems provides many advantages in the implementation of wireless systems, one of its main disadvantages is its sensitivity to phase noise, which is a random process caused by fluctuations of the transmitter and receiver oscillators [26] and time-selective fading. Both phase noise and time-selective fading destroy the orthogonality among subcarriers, causing inter-carrier interference (ICI). Many future-generation wireless systems will use higher frequency bands (e.g., 60 GHz radio). Voltage-controlled oscillators (VCO) with low phase noise operating at these frequencies, although feasible [27], are usually expensive. Alternatively, such a high-frequency carrier could be generated by multiplying the output of a VCO operating at relatively low frequency with a reference signal at a frequency close to the carrier frequency. In this case, both phase noise and fading rapidity scale up linearly relative to the conventional radios (e.g., those operating at 5 GHz).

Depending on whether the local oscillator is a phase-locked loop (PLL) or is frequency-locked (free-running), phase noise can be categorized by two different models. For the former, phase noise can be modeled as a zero-mean, stationary random process with finite power [29], whereas for the latter, phase noise is a zero-mean, nonstationary Wiener process with infinite power. As suggested in [28], even though the phase noise process cannot always be assumed as stationary, the phase noise disturbance can be. The phase noise effects can be reduced to a certain extent by improving the performance of the local oscillator itself; however, this could be costly. Hence, it is important to develop simple, low-complexity alternatives to expensive VCOs.

The effects of phase noise have been analyzed extensively by existing work, which generally consider time-invariant channels. In [26], the bit-error-rate (BER) sensitivity of OFDM systems over AWGN channels is analyzed, where phase noise is assumed to be a Wiener process. Similarly in [30], the effects of the Wiener phase noise on different modulation schemes for OFDM systems are characterized. In [31], the dependence of phase noise effects on subcarrier spacing is studied and in [32] this analysis is extended to study the system performance with varying numbers of subcarriers. A general analysis that unifies and extends previous results is provided in [28]. In [29], a feed-forward phase noise correction method based on pilot subcarriers is presented. A method to suppress the phase noise employing a minimum-mean square error (MMSE) equalizer and assuming quasi-static fading for multiple-input multiple-output (MIMO) wireless local area networks (WLAN) is presented in [33]. In [34], a blind detection method in the presence of PLL phase noise is provided based on the expectation-maximization (EM) technique; however, no fading model is considered and the phase noise is modeled as the output of an autoregressive moving average (ARMA) system driven by a white Gaussian noise, which is not an exact model.

In Chapter 4, a ML phase-noise estimation and suppression scheme is derived. This part of the thesis also focusses on wireless systems that employ the OFDM scheme.

1.1.4. Predictive Base Station Switching for Broadband Wireless Systems

Broadband wireless access (BWA) systems such as WIMAX (i.e. IEEE 802.16e [10]) are expected to support high-mobility mobile stations (MS). High-data-rate transmission requires strong received signal levels; thus micro-cells or pico-cells are commonly deployed for BWA. Traditional handover decision algorithms developed for mobile cellular communications usually result in an excessive number of handovers, when applied to BWA micro- or pico-cell systems, due to possible high user speeds and smaller cell sizes. This will be a setback for handover schemes that require considerable amount of network resources since there will be a significant handover overhead, resulting in a reduced overall network throughput. In addition, the delay caused by the handover process might be a problem for delay-sensitive applications. Although faster handover algorithms have previously been proposed [39], the ideal solution to reduce handover delay and overhead is to minimize the number of handovers while maintaining the received signal level.

Most of the existing handover algorithms are developed for mobile cellular systems that operate in macro-cell configurations and that have less restrictive bit-error-rate (BER) requirements compared to BWA systems. Hence, minimizing the number of handovers is far more critical for micro-cell or pico-cell networks. Mobile speed and traveling direction information, when appropriately exploited, could help increase the efficiency of handover algorithms. In [40], a method based on the maximum Doppler frequency to dynamically change the measurement intervals for handoff decisions based on mobile speeds is provided, and a similar but more comprehensive work can be found in [41]. An algorithm employing global positioning system (GPS) with a hysteresis parameter that is regulated based on the distance between the MS and surrounding base stations (BS) is presented for wideband code-division multiple-access systems in [42]. Similarly, in [43], a soft handover scheme based on dynamically adjusted hysteresis values based on the MS direction is presented, where a BS to which the MS is approaching is favored over a BS from which the MS is receding. A seamless handoff architecture with an integral movement tracking algorithm can be found in [44], where the direction is estimated from the location measurements of the MS. The direction information is used to decide on the movement patterns: linear, stationary, or stochastic.

The goal of Chapter 5 is to develop a new handover algorithm, called predictive base station switching (PBSS), which will dramatically reduce the handover rate without degrading the received signal levels. This is achieved by utilizing the mobile speed and direction information. This algorithm can be used for hard handover schemes to decide the new target BS, for soft handover schemes to select the new anchor BS, and even for softer handover schemes to create a connection with an active BS in the diversity list.

Chapter 5 mainly focusses on WAN systems (especially WIMAX).

1.2. Contributions

1.2.1. Contributions provided by ML Maximum Doppler Frequency Estimation

This algorithm presented in Chapter 3 is a frequency-domain approach which can be readily applied to any OFDM system as it is based on the already-existing pilot subcarriers, and hence it does not cause additional system overhead as mid-amble based algorithms. The estimator can be implemented as a low-complexity, finite impulse response (FIR) filter bank, whose coefficients can be pre-calculated and conveniently stored in the system memory.

It is well known that time-varying fading causes intercarrier interference (ICI) in OFDM systems. However, existing work on Doppler estimation has not properly modeled ICI effects. A novel ICI model is provided taking into consideration its effects for accurate estimation results in order to avoid an error floor. The algorithm accommodates different choices of design parameters, allowing flexible performance-complexity tradeoffs. The Cramér-Rao lower bound is also derived for the presented algorithm.

1.2.2. Contributions provided by ML Phase Noise Suppression

Main contributions provided by the work presented in Chapter 4 are as follows:

(a) The *fast* time-varying aspect of the channel is incorporated, and the effect of ICI is included in the phase noise suppression. While this type of modeling is more practical, a great majority of the existing works only consider time-invariant, or quasi-static channels. As will be shown in Section 4.4, when both fast time-varying fading and phase noise are considered, the effect of the phase noise, unlike the case for time-invariant fading channels, cannot be readily separated from the channel coefficients and data symbols to be presented as a simple common phase error (CPE) term. To make the analysis and suppression of phase noise tractable, an approximation to the phase noise is presented with justification.

(b) The method provided is valid for both the phase-locked and free-running cases.

(c) Phase noise correction is performed without assuming perfect channel equalization, whereas in much of the prior work, the channel is assumed to be known prior to the phase noise suppression, which is not realistic. The phase noise estimation is performed using the pilot subcarriers that are embedded in practical OFDM systems. The major components to implement the proposed ML approach can be stored in the system memory for reduced complexity.

(d) A doubly-selective fading environment is considered rather than assuming a time-invariant and/or flat-fading channel.

1.2.3. Contributions provided by Predictive Base Station Switching

The algorithm proposed in Chapter 5 differs from existing algorithms based on direction and speed in many ways:

(a) It employs signal measurements and MS-BS distance to decide whether a handover is necessary.

(b) A decision metric is calculated for each BS, considering the fact that even if the MS is approaching two base stations, the MS might remain connected to one of them much longer than the other one.

(c) The length of the prediction step is variable and is based on the MS speed.

(d) The degradation in the received signal levels as a result of using PBSS is negligible, and

(e) It does not require a movement pattern.

It is demonstrated via simulation results that even when the MS moves randomly or when the direction information is not available, the PBSS performance is still better than classical schemes based only on signal strengths and MS-BS distance information.

1.3. Notation Summary

Acronyms and mathematical notations are listed below.

Notation	Description
AWGN	Additive White Gaussian Noise
BER	Bit Error Rate
BS	Base Station
BWA	Broadband Wireless Access
CBSS	Classic Base Station Switching
CPE	Common Phase Error
CRB	Cramer-Rao Bound
FBSS	Fast Base Station Switching
FFT	Fast Fourier Transform
GPS	Global Positioning System
HHO	Hard Handover
ICI	Intercarrier Interference
i.i.d.	Independent and identically distributed
ISI	Inter-symbol Interference
MDHO	Macro Diversity Handover
ML	Maximum Likelihood
MLE	Maximum Likelihood Estimation
MMSE	Minimum Mean-Square Error
MS	Mobile Station
MSE	Mean-Square Error

OFDM	Orthogonal Frequency Division Multiplexing
PAN	Personal Area Networks
PBSS	Predictive Base Station Switching
PSD	Power Spectral Density
QPSK	Quadrature Phase-Shift Keying
SHO	Soft Handover
SNR	Signal-to-Noise Ratio
WAN	Wide-Area Networks
WLAN	Wireless Local Area Networks
WIMAX	Worldwide Interoperability for Microwave Access
$J_0(\cdot)$	Zeroth-Order Bessel Function of the First Kind
$(\cdot)^H$	Complex Conjugate Transpose
f_d	Maximum Doppler Frequency
f_dT	Normalized Maximum Doppler Frequency
$\phi(n)$	Phase Noise
$\theta(n)$	Phase Noise Disturbance
P_{dir}	Probability of Direction Change
v_{MS}	MS speed
R_{BS}	Effective Base Station Range
P_{BS}	Expected time MS will be connected to a certain BS
t_{BS}	Time MS spends in R_{BS}
$\overline{d}_{\mathrm{BS}}$	Average MS-BS Distance
λ_{BS}	Base Station Decision Metric

2. OVERVIEW OF OFDM SYSTEMS AND CHANNEL MODEL

Since most of the research findings in this thesis are closely related to orthogonal frequency division multiplexing (OFDM) systems, OFDM systems will be reviewed in this chapter. In addition, given that the research presented in this thesis is on wireless systems, it is also crucial to reassess the model for the medium in which wireless signals travel, namely, the channel model.

2.1. OFDM System Description

The review on OFDM systems presented in this section will not be very profound, however it will not be brief either. The intent of this chapter is to make a reader not familiar with OFDM systems but has good knowledge in Signal Processing and Telecommunications Theory to understand the rest of the thesis and the underlying reasoning behind the algorithms presented in this thesis.

As presented in Chapter 1, wireless standards are going through an evolution, with a focus on broadband, IP-centric platforms rather than legacy narrowband, circuit-switched systems. Due to its advantages in high-speed communications, as it will be presented later in this chapter, OFDM has become the modulation scheme of choice for a number of high profile wireless systems.

The reason for the strong presence of OFDM in many broadband wireless systems lies in the fact that it transmits high-data rates via multiple parallel low-rate frequency-domain streams, and provides increased robustness to multiple-access interference (MAI) and the effects of multipath channels. OFDM therefore offers an excellent performance over frequency selective and interfered channels.

The notion of frequency-division multiplexing (FDM) can be dated back at least half a century. Early OFDM systems have first been proposed for military applications by Bello [11], Zimmermann [12] and other researchers. High spectral efficiency and low cost implementation of FDM became possible in the 1970s and 1980s with advances in Digital Fourier Transform (DFT), however one had to wait until 1990s to witness the first OFDM-based wireless system, which was the Digital Audio Broadcasting (DAB) standard of the European Telecommunications Standards Institute (ETSI) [13].

The main reason OFDM has become so preferred lies in its intrinsic design properties. Wireless systems have to cope with many different types of *interference*. Main interference sources that arise from the physical medium can be considered to be the *channel fading* (both time and frequency selective, or the so-called *doubly-selective* channels); and multiple-access interference (MAI), arising from the interference of other users using the same system and hence the same spectrum.

The basic idea behind an OFDM system is to use orthogonal subcarriers in the frequency domain to transmit data in parallel over the channel. Each OFDM symbol is associated with a certain number of orthogonal carriers in the frequency domain. The total throughput of the system then becomes the sum of the throughput of all subcarriers.

One of the main advantages of OFDM is its ability to convert dispersive broadband channels into parallel narrowband subcarriers, thus significantly simplifying the channel equalization at the receiver end. Another important property of OFDM is its flexibility in allocating different power levels among different subcarriers. This capability is particularly important for broadband frequency-selective channels; if one subcarrier is faded more severely than others, it might either be discarded, or in some cases, a higher power can be allocated to that specific subcarrier. It should be noted, however, that subcarrier-based power adjustment is less feasible than neglecting significantly-faded subcarriers.

Some subcarriers of an OFDM symbol are reserved for pilot carriers, which are used for many different purposes, including channel estimation. In Chapters 3 and 4, these pilot carriers are actively used both to estimate the maximum Doppler frequency and to suppress the phase noise introduced by the local oscillator. Also, to avoid adjacent channel interference, the subcarriers at the beginning and end of the OFDM spectrum are non-active carriers and do not carry any information bits.

Another strong point of OFDM is its property to easily cope with inter-symbol interference (ISI), which is the interference of the previously sent symbol onto the current symbol due to multipath channels. Generally, the effects of ISI are corrected at the receiver. However, if the system is immune to ISI, as in the case for OFDM, it would be possible to reduce the receiver cost. OFDM uses a cyclic prefix to successfully cope with ISI.

The basic idea behind a cyclic prefix is to add a *prefix* to the beginning of an OFDM symbol in the time domain, which is discarded at the receiver. This discarded cyclic prefix is the part that is most effected by ISI. The length of the cyclic prefix is a design parameter. It should not be less than the channel memory (i.e. channel delay spread), however, as it is not used to carry any data, a very long cyclic prefix would cause significant decrease in the system throughput.

It is also important to note why this prefix is made cyclic. If instead of a cyclic prefix, a zero-padding prefix was used, as in Fig. 2.1 [13], the integrity of the signal could not have been maintained. To be able to analyze the relationship between the transmitted and received signals, the perfectly accurate linear model can be used for multipath channels, which can be written in continuous time as

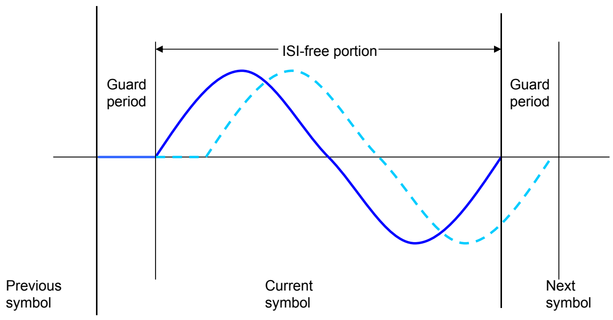

FIGURE 2.1. Figure depicting the zero-padding prefix option for OFDM guard interval.

$$y(t) = h(t) * x(t) = \int_{-\infty}^{\infty} h(t)x(t-\tau)d\tau \tag{2.1}$$

where, $h(t)$ can be considered as the channel response and $x(t)$ can be considered as the transmitted signal. If $x(t)$ is considered to be a complex exponential in the form of $x(t) = se^{jwt}$ (where s is the magnitude of $x(t)$), than the received signal $y(t) = sH(jw)e^{jwt}$ would be a scaled version of the input (where $H(jw)$ is the continuous-time Fourier transform of $h(t)$), as complex exponentials are eigenfunctions of linear systems. This is generally true for infinitely long exponentials, but also if the channel impulse response can be modeled as finite-impulse response (FIR). So, from the perspective of OFDM systems, if the prefix is made to be cyclic as in Fig. 2.2 [13], linear convolution can be considered as a circular convolution as long as the channel delay spread is less than the allocated guard interval [14].

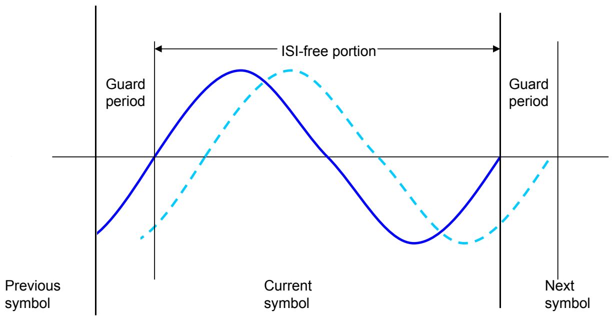

FIGURE 2.2. Figure depicting the cyclic prefix option for OFDM guard interval, which turns linear convolution into circular convolution.

Before discussing further the advantages and drawbacks of OFDM systems, a very simplistic representation of OFDM scheme is depicted in Fig 2.3. In this schematic, the pilot carriers, the active data carriers, and inactive carriers are demonstrated. Furthermore, the use of inverse fast Fourier transform (IFFT) to obtain the time domain signal to be transmitted, as well as, the creation of the cyclic prefix is illustrated. In the transmitter, a serial-to-parallel converter is used to obtain data for each active carrier before obtaining the time-domain signal.

When the signal is received at the receiver, channel equalization and time/frequency synchronization is initially performed. Then, the cyclic prefix of the OFDM symbol is discarded, and the received signal is converted back to the frequency-domain via the use of a block FFT. After these steps, the data that is carried by each subcarrier can be obtained, and a parallel-to-serial converter can be employed to reconstruct the exact sequence that was sent.

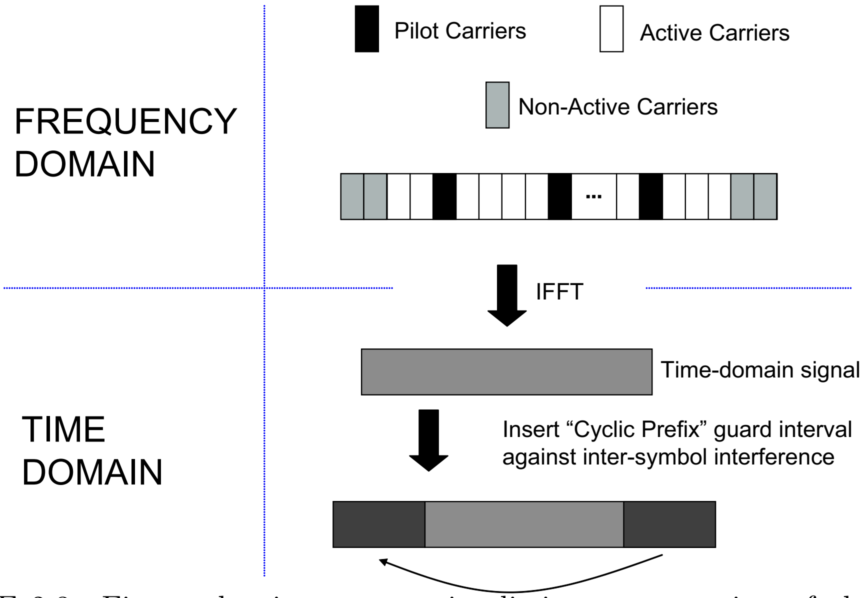

FIGURE 2.3. Figure showing a very simplistic representation of the OFDM scheme and its carriers.

Of course, in all realistic systems, channel coding/decoding blocks, interleaving/deinterleaving blocks, and transmit/receive filters are employed to improve the system performance. Radio frequency (RF) modulator/demodulator and RF amplifiers are also used to convert the baseband signal to the appropriate frequency band imposed by the standard [15]. In much of the simulations in this thesis, the OFDM signal is processed at the baseband, as the effects of RF modulation and demodulation are clearly documented in the literature and they are beyond the scope of this thesis.

TABLE 2.1. Advantages and drawbacks of OFDM systems.

Main Advantages	**Main Drawbacks**
High Spectral Efficiency	Sensitivity to ICI
Simple Implementation	High Peak-to-Average Power Ratio
Resistance to frequency-selective fading	Sensitivity to phase noise

2.1.1. Advantages and Drawbacks of OFDM systems

Table 2.1 provides the main advantages and drawbacks of OFDM systems. Of course, as it is with many other communication systems, the most appropriate system should be chosen depending on the application. OFDM provides some major advantages and the effects of some of its drawbacks can be reduced. For example, Chapter 4 of this thesis focuses on suppressing the phase noise in order to improve the overall system performance.

2.1.1.1. Advantages of OFDM systems

High spectral efficiency: OFDM is a highly efficient modulation scheme which has been shown to approach the information theoretical capacity when water-filling is applied across its subcarriers. Especially adaptive coded modulation, which is coding different OFDM subchannels (each subchannel is composed of a group of subcarriers), has been implemented in some IEEE standards [13].

Simple implementation: OFDM can be easily implemented via the use of FFT and IFFT blocks. As these blocks are easily available and their complexity and hence power consumption is relatively lower, the implementation simplicity of OFDM is definitely a major plus.

Resistance to fading and interference: As described before, OFDM is immune to multipath effects due to the use of a cyclic prefix. This is definitely an advantage of OFDM systems, as it greatly simplifies the design of receiver structure.

2.1.1.2. Drawbacks of OFDM systems

The two main disadvantages of OFDM systems are their sensitivity to time/frequency synchronization and the very high peak-to-average power ratio. The most important characteristic of OFDM systems is that individual carriers of an OFDM symbol in the frequency-domain are orthogonal to each other at the center of a subcarrier as shown in Fig 2.4. However, while estimating the carrier frequency, if a small error of δf is committed, the orthogonality of individual carriers will not hold true anymore. Furthermore, since the maximum of the *sinc* function does not occur at $f_n + \delta f$ but at f_n, there will also be a decrease in the magnitude of the sample of carrier n. This fact is shown in Fig. 2.5.

As this effect is caused by the *interference* of neighboring subcarriers, it is called intercarrier interference (ICI). Considering the number of subcarriers is large enough, this interference can be modeled as a Gaussian random process through the central limit theorem. Another important point to mention here is that those carriers that are closest to the center of the allocated frequency band of the system will be effected more by ICI.

ICI is not only caused by frequency synchronization errors; time-varying fading environments, as well as phase noise, might also cause ICI as will be investigated in Chapter 4.

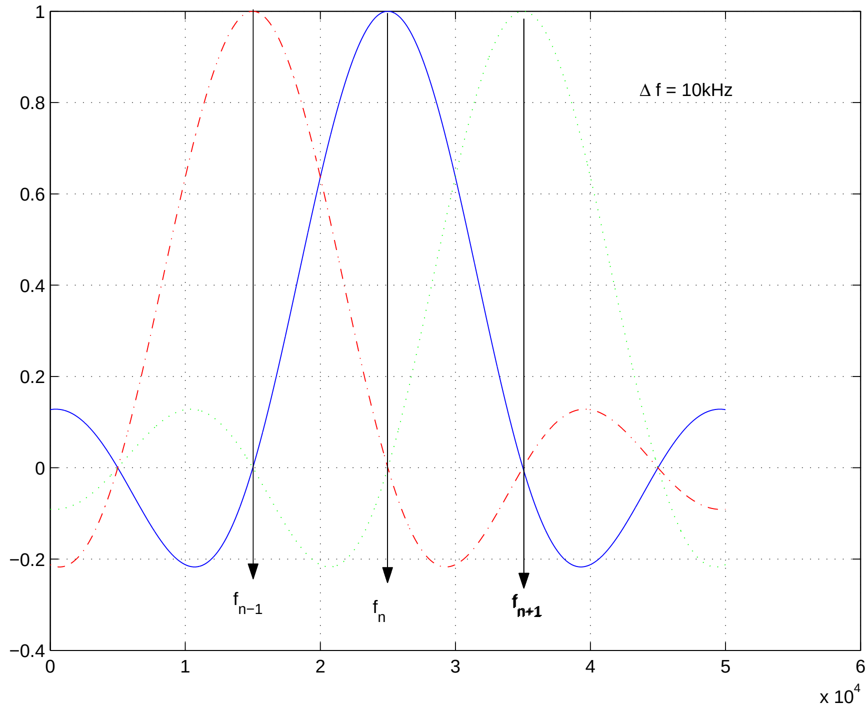

FIGURE 2.4. Figure showing the orthogonality among different OFDM carriers when $\Delta f = 10kHz$.

The second important problem of an OFDM system is the high peak-to-average power ratio, as mentioned before. An OFDM signal can be considered as a superposition of many sinusoidal signals, hence its mean power is very small compared to the peak power. This creates a difficulty when the signal needs to be amplified for transmission, or for processing at the receiver side. If the transmit or receive amplifier does not have a large dynamic range, then the signal will be clipped, which will cause a significant data loss. A similar problem will occur if the power amplifier is not linear [16]. Thus, OFDM systems generally require expensive power amplifiers, which drive the unit costs up.

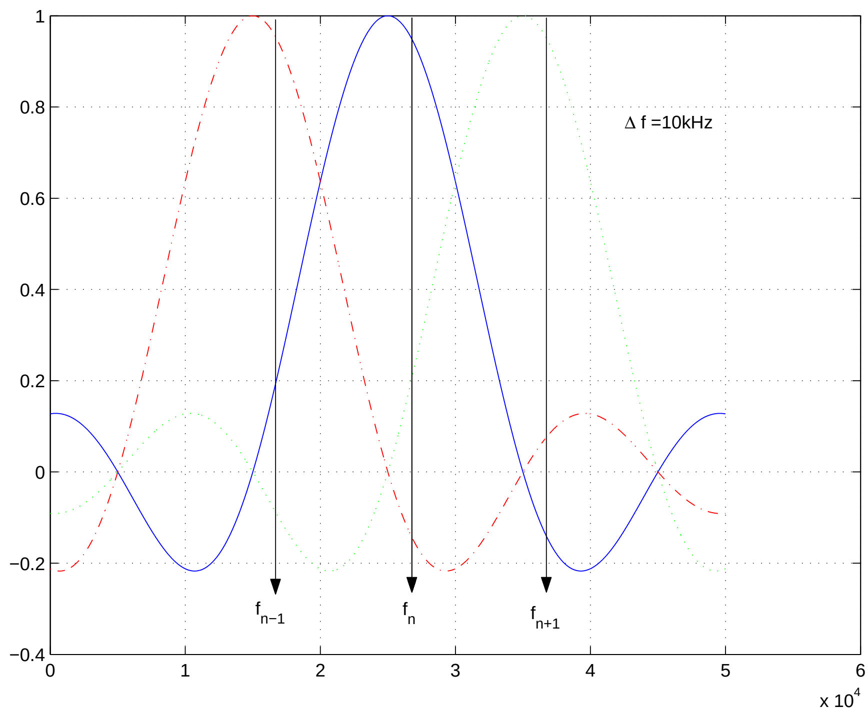

FIGURE 2.5. The loss of orthogonality due to the intercarrier interference is shown when $\Delta f = 10kHz$.

2.2. Channel Model

In this section, the channel model is described. Basically, the channel model can be divided into two categories. The first category captures the large-scale propagation effects, which mainly characterize the channel behavior over large transmitter-receiver separation distances. This category is used to define, for example, the coverage area of a certain transmitter. Main large-scale propagation effects considered in this thesis are path loss and shadowing. This type of channel characterization is used in Chapter 5.

The second category encompasses the propagation models that are used to characterize rapid fluctuations of the channel. This category is generally addressed as small-scale propagation effects, or fading models [17]. In this category, the channels can be distinguished based on their time-variance properties (fast or slow), or based on their multipath time delay spread properties (flat or frequency-selective). This type of channel characterization is employed in Chapters 3 and 4.

2.2.1. Large-scale Propagation Effects

As wireless signals are transmitted, they become reflected, scattered and diffracted by the surrounding environment. Even if there are no obstacles between the transmitter and the receiver (i.e. in a line-of-sight (LOS) environment), there will be a difference between the received signal power, P_r, and the transmitted signal power, P_t, which is called the free-space path loss [17]. Free-space path loss is inversely proportional to the square of the distance between the transmitter and the receiver, d, and is proportional to the wavelength of the carrier, λ

$$\frac{P_r}{P_t} = \left[\frac{G\lambda}{4\pi d}\right]^2, \tag{2.2}$$

where G is the product gain of the transmit and receive antenna field radiation patterns in the LOS direction [8].

However, considering that most wireless systems operate in dense-urban, urban, or suburban areas, it is expected that the actual path loss will be very different and more complex than the assumption of Eq. 2.2. For a specific situation, it is possible to calculate the exact path loss model using ray tracing. However, this is not feasible as it is impossible to perform ray tracing for an infinite number possible scenarios for each wireless system. To solve this problem, a number of empirical path loss models have been developed for a variety of environments.

Even so, these models might not fit perfectly the nature of a specific environment, as they are based on approximations [8].

It should be clear at this point that due to the complexity of the path loss mechanism, it is impossible to obtain a single model that clearly represents path loss in different environments. However, as presented in [8] and [17] for a basic tradeoff calculation, a *simplified* path loss model can be derived, which captures the essence of signal propagation and prevents the need to resort to complicated path loss models. Such a model is presented in Eq. 2.3.

$$P_r = P_t K \left[\frac{d_0}{d}\right]^{\gamma}, \tag{2.3}$$

where d_0 is the reference distance, K is a unitless constant that is based on the antenna characteristics (at a known distance d_0) as given in Eq. 2.4 in dB, and γ is the path loss exponent, which is ranges from 1.5 to 6, depending on the environment.

$$K = 20 \log \frac{\lambda}{4\pi d_0}. \tag{2.4}$$

The constant K can be replaced by accurate measurement results, if such results are available at a specific d_0.

Another important notion to consider regarding large-scale propagation effects is shadowing, which is caused by the blockage created by natural or urban obstacles and results in variations in the received power level. This blockage effect is called *shadowing*, and it degrades the actual received power level. The combined path loss and shadowing effect is depicted in Fig. 2.6 [8].

The shadowing effect is modeled randomly, and the i-th obstacle is considered to have a depth of d_i and an attenuation constant of α. The attenuation effect caused by the i-th obstacle can then be modeled as

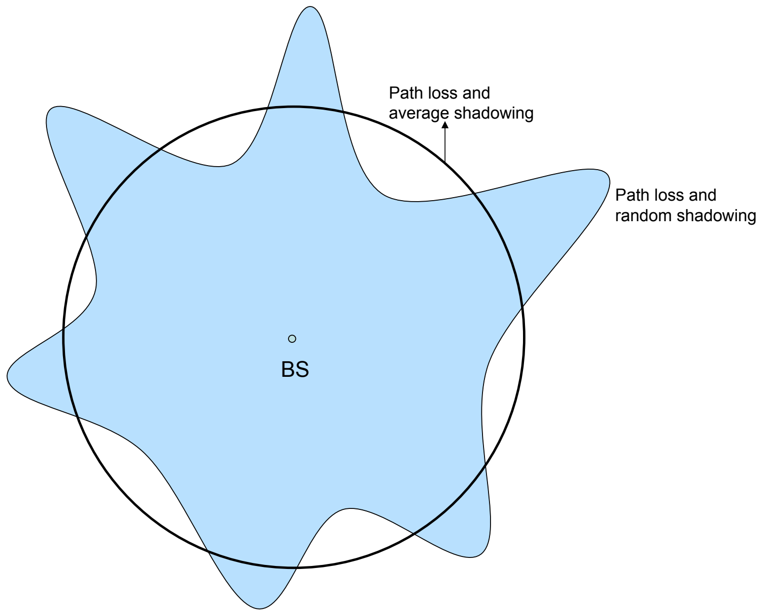

FIGURE 2.6. Figure showing the combined effect of path loss with random and average shadowing.

$$s_i = e^{-\alpha d_i} \tag{2.5}$$

where it is assumed that all the obstacles have the same attenuation constant. Considering there are a total of D such obstacles, their combined shadowing effect, s, can be written as in Eq. 2.6.

$$s = e^{-\alpha \sum_{i=0}^{i=D-1} d_i} = e^{-\alpha d_t} \tag{2.6}$$

where, $d_t = \sum_{i=0}^{i=D-1} d_i$. Assuming the number of obstacles, D, is large, the central limit theorem can be used to approximate d_t as a Gaussian random variable. This fact would allow us to consider the shadowing effect, when expressed in dB, to be a Gaussian random variable with mean μ_s and standard deviation σ_s [8].

2.2.2. Small-Scale Propagation Effects (Fading Models)

The propagation models that characterize the rapid fluctuations of the received signal power level over short distances or short time durations are called small-scale propagation effects or fading models [17]. Such channels have two different categories. They can be categorized as either flat-fading or frequency-selective, depending on the coherence bandwidth, and fast or slow time-varying, depending on the coherence time. A channel model that is both frequency-selective and fast time-varying is considered to be a doubly-selective channel.

2.2.2.1. Flat or Frequency-Selective Channels

The multipath effect is the result of the reflections from the surrounding natural or urban structures. Due to the presence of these structures, a signal sent from the transmitter will arrive at the receiver following many different paths, hence the name *multi*path. Each of these signals arrive at the receiver at different times, depending on the amount of time it takes them to travel their specific path.

If it is not factored into the receiver processing, the multipath effect can degrade the signal performance. However, these multipath signals can also be used for extra diversity, as each of them are copies of the same transmitted signal. To be able to use this diversity, different multipath signal should be temporally *resolvable*, i.e. their difference in arrival time to the receiver should be greater than the inverse of the signal bandwidth.

To be able to define whether a channel is flat or frequency-selective, one can make use of the rms (root-mean-square) delay spread. The rms delay spread is basically the standard deviation of the delay of different multipath signals, weighted with respect to their energy. The inverse of the rms delay spread is proportional to the *coherence* bandwidth. If the bandwidth of the transmitted signal is less than the coherence bandwidth, the channel can be considered flat. On the other hand, if the signal bandwidth is larger than this value, then the signal components at different frequencies will be faded differently, hence the name, frequency-*selective*. From the perspective of time-domain effects in frequency-selective channels, the transmitted symbols are spread in time, which introduces intersymbol interference, or ISI.

2.2.2.2. Fast or Slow Time-varying Channels

A channel can be characterized as fast time-varying, if the symbol duration of a signal is greater than the coherence time of the channel. Otherwise, it is considered to be slow time-varying. The coherence time can be considered as the inverse of the Doppler spread, which is the width of the Doppler spectrum; and the Doppler spectrum is the Fourier transform of the autocorrelation function of the received signal.

The relative motion between the transmitter and the receiver creates different Doppler shifts. These shifts will be positive if the two are moving towards each other, and it will be negative if they are moving away from each other. Furthermore, in a multipath channel, the surrounding objects that are in motion can also change the nature of the Doppler shifts, especially if they are moving at a speed comparable or greater than the relative speed of the transmitter and the receiver. In case these Doppler shifts result in a wider Doppler spread, the channel coherence time will decrease, and the channel can be considered to be even *faster* time-varying.

3. A ML MAXIMUM DOPPLER FREQUENCY ESTIMATOR FOR OFDM SYSTEMS

3.1. System Description

We consider an OFDM system with K active subcarriers and FFT length N, where $K \leq N$. Let N_G denote the length of the guard interval, or cyclic prefix, and $d_k,\ k = 1, 2, \ldots, K$, represent the data transmitted over the k^{th} data subcarrier. The transmitted OFDM signal in the time domain can then be expressed as

$$x(n) = \sqrt{\frac{E_s}{N}} \sum_{k \epsilon \mathcal{K}} d_k e^{j2\pi nk/N}, \quad - N_G \leq n \leq N - 1 \tag{3.1}$$

where E_s is the symbol energy per subcarrier, $\mathcal{K}$ represents the set of active subcarriers, or subcarriers carrying information data, and $E\{|d_k|^2\} = 1$. Without loss of generality, we assume that the active subcarriers are from 0 to $K-1$. Then Eq. (4.3) can be rewritten as

$$x(n) = \sqrt{\frac{E_s}{N}} \sum_{k=0}^{K-1} d_k e^{j2\pi nk/N}, \quad - N_G \leq n \leq N - 1. \tag{3.2}$$

We consider a time-varying Rayleigh fading channel with a maximum delay of T_d and an rms delay spread τ_{rms}. The channel is described using a tapped delay line model with an exponentially decaying tap power. We assume that $T_d \leq N_G$, and that the autocorrelation of the inverse Fourier transform of the Doppler spectrum can be modeled by a zeroth-order Bessel function of the first kind. The channel coefficient of the l-th tap $(0 \leq l \leq T_d - 1)$ at time n is denoted as $h_l(n)$. By stacking vertically all the T_d channel coefficients at time n, we obtain

$$\boldsymbol{h}(n) = [h_0(n)\ h_1(n)\ \cdots\ h_{T_d-1}(n)]^T \tag{3.3}$$

where $[\cdot]^T$ stands for transpose.

We further assume that the channel taps (i.e., elements of $\boldsymbol{h}(n)$) are independent and identically distributed (i.i.d.), zero-mean, circularly symmetric complex Gaussian random variables. The channel autocorrelation function is expressed as

$$E\{\boldsymbol{h}(n+\Delta n)\boldsymbol{h}^H(n)\} = cJ_0\left(\frac{2\pi f_d T \Delta n}{N}\right)\boldsymbol{E} \tag{3.4}$$

where $(\cdot)^H$ denotes complex conjugate transpose, c is a scaling factor which is used to normalize the channel power, T is the duration of N samples, $J_0(\cdot)$ represents the zeroth-order Bessel function of the first kind, and $\boldsymbol{E}$ is a diagonal $T_d \times T_d$ matrix whose l-th diagonal entry is $e^{-l/\tau_{rms}}, \quad 0 \leq l \leq T_d - 1$. The earlier assumption that the guard interval N_G is not less than the multipath spread ensures ISI-free operations. Our objective is to accurately estimate the normalized maximum Doppler frequency $f_d T$ based on the received signal using pilot subcarriers.

3.2. ML Maximum Doppler Frequency Estimator

The received signal through a time-varying multipath channel can be written as

$$y(n) = \sum_{l=0}^{T_d-1} h_l(n)x(n-l) + \omega(n) \tag{3.5}$$

where $\omega(n)$ is the additive white Gaussian noise (AWGN) with zero-mean and variance σ_ω^2. We assume without loss of generality that $E_s = 1$; thus the variance of the AWGN equals the inverse of the signal-to-noise ratio (SNR), i.e., $\sigma_\omega^2 = 1/\text{SNR}$. Once an OFDM symbol is received, the guard interval (the first N_G samples) is discarded, leaving the ISI-free data portion. The received signal during the data portion is expressed as

$$y(n) = \frac{1}{\sqrt{N}} \sum_{k=0}^{K-1} d_k e^{j2\pi nk/N} H_k(n) + \omega(n) \tag{3.6}$$

where $H_k(n) = \sum_{l=0}^{T_d-1} h_l(n) e^{-j2\pi lk/N}$. The data signal on the k-th subcarrier of an OFDM symbol at the FFT output is expressed as [24]

$$\begin{aligned} Y_k &= \frac{1}{\sqrt{N}} \sum_{n=0}^{N-1} y(n) e^{-j2\pi nk/N} \\ &= d_k H_k + \alpha_k + W_k \end{aligned} \tag{3.7}$$

where

$$H_k = \frac{1}{N} \sum_{n=0}^{N-1} H_k(n) \tag{3.8}$$

$$\alpha_k = \frac{1}{N} \sum_{m=0, m\neq k}^{K-1} d_m \sum_{n=0}^{N-1} H_m(n) e^{j2\pi n(m-k)/N} \tag{3.9}$$

$$W_k = \frac{1}{\sqrt{N}} \sum_{n=0}^{N-1} w(n) e^{-j2\pi nk/N}. \tag{3.10}$$

The term α_k represents the ICI component. The power of ICI may be negligible when the maximum normalized Doppler frequency f_dT is small (e.g., $f_dT < 0.02$) [24], but ICI should be considered for the general case. Although the ICI power is guaranteed to be small enough in most applications in OFDM systems, the Doppler frequency information can be extracted from the ICI component. Thus, we will include the ICI term in the ML formulation. To allow the use of more than one OFDM symbols to estimate the maximum Doppler frequency, we assume that certain amount of latency is acceptable. When multiple OFDM symbols are considered, we can rewrite Eq. (3.7) by including the index n denoting the n-th OFDM symbol as

$$Y_{k,n} = d_{k,n}H_{k,n} + \alpha_{k,n} + W_{k,n}. \tag{3.11}$$

Let $\mathcal{P}$ represent the set of pilot subcarriers. Since the values $d_{k,n}$, $k \in \mathcal{P}$, are known, the noisy estimate of the channel can be obtained as

$$\begin{aligned}\tilde{H}_{k,n} &= \frac{Y_{k,n}}{d_{k,n}} \\ &= H_{k,n} + \alpha_{k,n}/d_{k,n} + W_{k,n}/d_{k,n}.\end{aligned} \tag{3.12}$$

This process can be done for all pilot subcarriers in the M consecutive OFDM symbols. From now on, we refer to a set of M consecutive OFDM symbols as an "estimation group.".

As illustrated in Fig. 3.1, using the specific pilot carrier k' of one estimation group, the vector $\boldsymbol{H}_{k'}$ can be obtained as

$$\tilde{\boldsymbol{H}}_{k'} = \left[\tilde{H}_{k',0}\ \tilde{H}_{k',1}, \cdots, \tilde{H}_{k',M-1}\right]^T. \tag{3.13}$$

The probability density function (pdf) of the ICI component $\alpha_{k,n}$ is a weighted Gaussian mixture pdf. However, through the central limit theorem, ICI can be

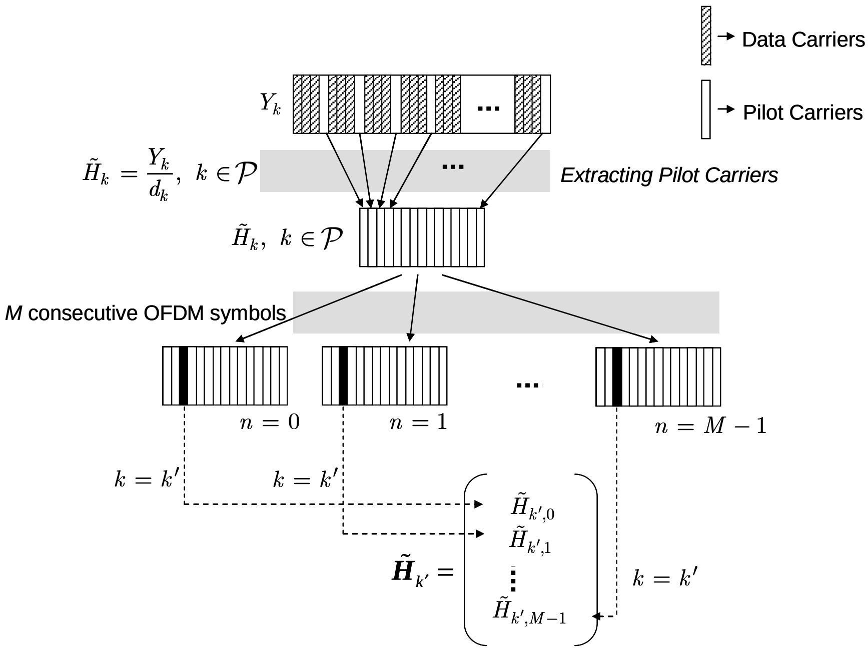

FIGURE 3.1. Detailed block diagram of $\tilde{\boldsymbol{H}}_{k'}$, $k' \in \mathcal{P}$.

approximated as a complex Gaussian random variable. Furthermore, as the ICI power is small enough compared to power of $H_{k,n}$, this Gaussian approximation would even hold if we could not have used the central limit theorem. In addition, when all subcarriers are pilot like in pre-amble and mid-amble, the ICI is a complex Gaussian random variable. Overall, it is safe to assume $\tilde{\boldsymbol{H}}_k$ as a zero-mean, circularly symmetric, complex Gaussian vector with the following pdf

$$p(\tilde{\boldsymbol{H}}_k) = \left[\pi^M \det(\boldsymbol{R})\right]^{-1} \exp\left(-\tilde{\boldsymbol{H}}_k^H \boldsymbol{R}^{-1} \tilde{\boldsymbol{H}}_k\right) \tag{3.14}$$

where $\boldsymbol{R}$ is the autocorrelation matrix of vector $\tilde{\boldsymbol{H}}_k$. The correlation of $H_{k,n}$ and $H_{k,n+\Delta n}$ was given in [24] as

$$E\{H_{k,n+\Delta n} H_{k,n}^*\} = \frac{1}{N^2} \sum_{l_1=0}^{N-1} \sum_{l_2=0}^{N-1} J_0\left(\frac{2\pi f_d T(l_1 + \Delta n N' - l_2)}{N}\right) \tag{3.15}$$

where $N' = N + N_G$. It is important to note that the above equation does not require the delay information. The correlation of the ICI term $\alpha_{k,n}$ in $\boldsymbol{R}$ can be derived as

$$E\{\alpha_{k,n+\Delta n}\alpha^*_{k,n}\} = \frac{1}{N^2}\sum_{\substack{m_1\neq k\\ m_1=0}}^{K-1}\sum_{\substack{m_2\neq k\\ m_2=0}}^{K-1} E\{d_{m_1,n+\Delta n}d^*_{m_2,n}\}$$
$$\sum_{l_1=0}^{N-1}\sum_{l_2=0}^{N-1} E\{H_{m_1}(l_1+\Delta nN')H^*_{m_2}(l_2)\}$$
$$e^{j2\pi(l_1+\Delta nN')(m_1-k)/N}e^{-j2\pi l_2(m_2-k)/N}. \tag{3.16}$$

The correlation term $E\{H_{m_1}(l_1+\Delta nN')H^*_{m_2}(l_2)\}$ in Eq. (3.16) is given by [24]

$$E\{H_{m_1}(l_1+\Delta nN')H^*_{m_2}(l_2)\} =$$
$$r_f(m_1-m_2)J_0\left(\frac{2\pi f_d T(l_1+\Delta nN'-l_2)}{N}\right). \tag{3.17}$$

where $r_f(m_1-m_2)$ represents the frequency-domain correlation

$$r_f(m_1-m_2) = c\sum_{l=0}^{T_d-1} e^{-l/\tau_{rms}}e^{-j2\pi l(m_1-m_2)/N}. \tag{3.18}$$

Finally, the correlation between the channel and the ICI component in $\boldsymbol{R}$ is given by

$$E\{H_{k,n+\Delta n}\alpha^*_{k,n}\} = \frac{1}{N^2}\sum_{\substack{m\neq k\\ m=0}}^{K-1} E\{d^*_{m,n}\}\sum_{l_1=0}^{N-1}\sum_{l_2=0}^{N-1} E\{H_k(l_1+\Delta nN')H^*_m(l_2)\}$$
$$e^{-j2\pi l_2(m-k)/N}. \tag{3.19}$$

From Eqs. (3.14)∼(3.19), the log-likelihood function can be obtained as

$$L(\tilde{\boldsymbol{H}}_k) = \ln(p(\tilde{\boldsymbol{H}}_k)) = \Omega - \ln(\det(\boldsymbol{R})) - \tilde{\boldsymbol{H}}_k^H\boldsymbol{R}^{-1}\tilde{\boldsymbol{H}}_k \tag{3.20}$$

where Ω is a constant term independent of the Doppler frequency. Maximizing the log-likelihood function is equivalent to minimizing the following cost-function

$$\Lambda_k(f_dT) = \ln(\det(\boldsymbol{R})) + \tilde{\boldsymbol{H}}_k^H \boldsymbol{R}^{-1} \tilde{\boldsymbol{H}}_k. \tag{3.21}$$

Hence, the maximum-likelihood estimate (MLE) of the normalized Doppler frequency can be obtained as

$$\widehat{f_dT} = arg \min_{f_dT} \Lambda_k(f_dT). \tag{3.22}$$

The MSE of an unbiased estimator is lower bounded by the Cramér-Rao bound [25], which can be found to be

$$\text{CRB} = \frac{1}{\Re\left\{tr\left[\frac{\partial \boldsymbol{R}}{\partial f_dT}\boldsymbol{R}^{-1}\frac{\partial \boldsymbol{R}}{\partial f_dT}\boldsymbol{R}^{-1}\right]\right\}} \tag{3.23}$$

where $\Re\{\cdot\}$ denotes the real part and $tr[\cdot]$ represents the matrix trace.

Exact calculation of the MLE requires the knowledge of delay profile. Since accurate delay profile may not be available in practical implementations, there might be a mismatch between the assumed $\boldsymbol{R}$ and actual $\boldsymbol{R}$; and the worst mismatch case occurs if the receiver assumes flat fading, i.e., $r_f(m_1 - m_2) = 1$. To better demonstrate the efficiency of the estimator, we also assume this worst case mismatch scenario throughout this chapter. However, for the theoretical Cramér-Rao bounds, we assume the delay profile is known and we employ the actual $\boldsymbol{R}$.

In order to improve the accuracy of the estimator, the MLE over multiple pilot subcarriers can be formulated. This requires the knowledge of statistics such as the channel delay spread and delay profile. Instead, we sum the cost function over pilot subcarriers as

$$\Lambda(f_dT) = \sum_{k\in\mathcal{P}} \Lambda_k(f_dT). \tag{3.24}$$

Further reduction in the MSE can be achieved in the time-domain by summing the cost function over more than one estimation groups at the expense of an increased latency. Although such time- and frequency-domain averaging of the cost function is not optimum, the performance of the estimator can be significantly improved.

For a specific estimation algorithm, the number of OFDM symbols in one estimation group, M, will be fixed. Thus, in order to significantly reduce the overall complexity of the system, the terms $\ln(\det(\boldsymbol{R}))$ and $\boldsymbol{R}^{-1}$ can be pre-calculated and stored in the memory for a certain range of normalized Doppler frequency values. The complexity can be further reduced since $\tilde{\boldsymbol{H}}_k^H \boldsymbol{R}^{-1} \tilde{\boldsymbol{H}}_k$ can be evaluated using a filter bank via Cholesky factorization and through low-rank approximation.

The main design parameters of the estimator are P, the number of pilot subcarriers from each OFDM symbol; M, the number of OFDM symbols in one estimation group; and G, the number of estimation groups. By choosing appropriate values for specific communications scenarios, we can achieve flexible performance-complexity tradeoffs. The performance, complexity, and the latency aspects under different parameters will be investigated by using simulations in the next section.

3.3. Simulation Results

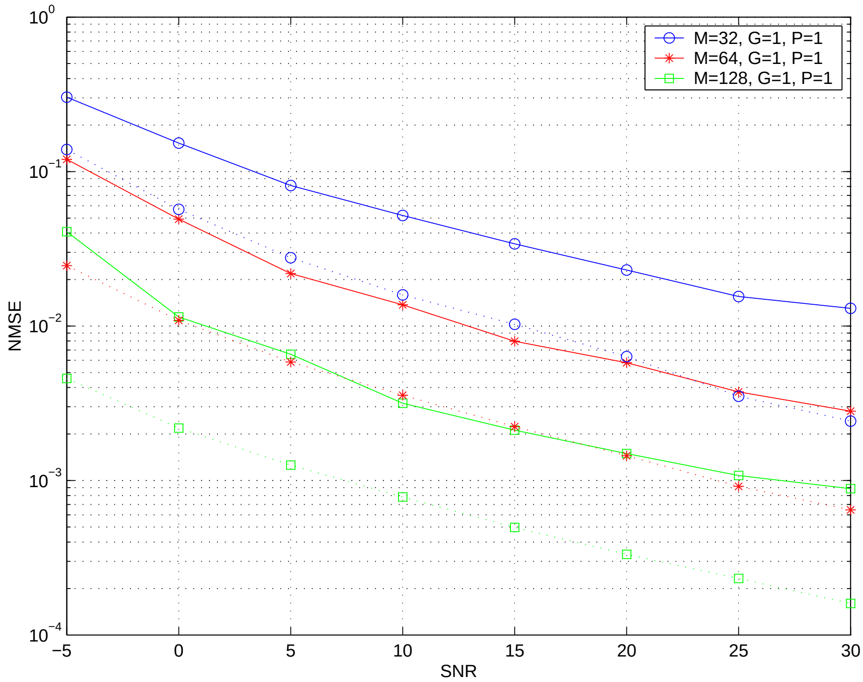

FIGURE 3.2. NMSE vs. SNR for different M when $G = P = 1$ (Solid: Simulation, Dashed: Cramér-Rao lower bound).

The time-varying channel is obtained by an FIR filter whose spectrum is the same as the one used in [24]. Each simulation is based on the observation of $50000 \times G \times M$ OFDM symbols. Without loss of generality, an OFDM symbol is assumed to have 32 subcarriers excluding the guard interval. The total length of an OFDM symbol including the guard interval is $112.5\mu s$, and the length of the guard interval is $12.5\mu s$. The maximum number of channel taps is assumed not to exceed the sample length of the guard interval, $N_G = 4$. The search range of the ML estimator is set to be $0 \sim 0.04$ with a step size of 0.001 (in terms of $f_d T$). We assume every one in four carriers is a pilot.

We define the normalized MSE (NMSE) as

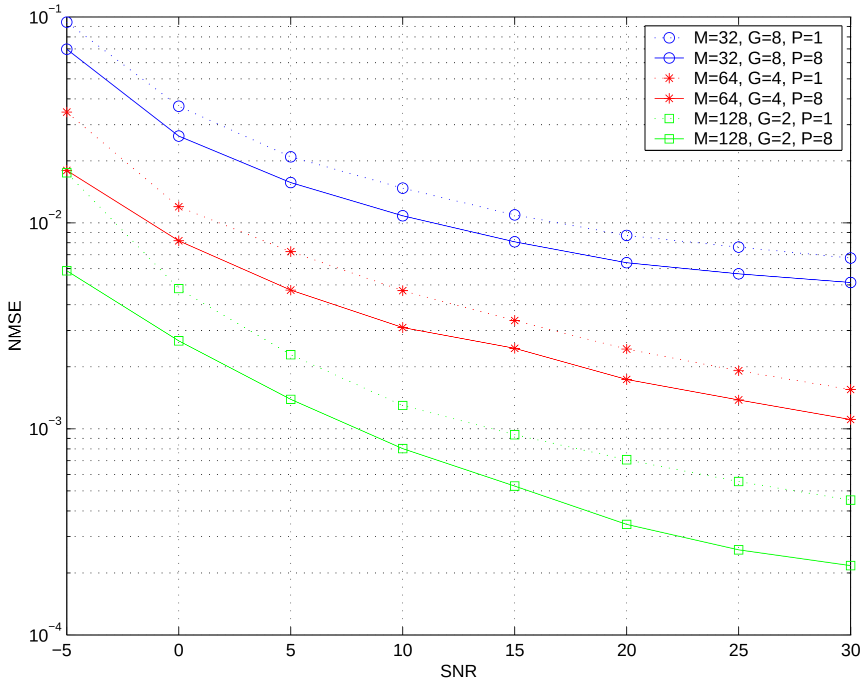

FIGURE 3.3. NMSE vs. SNR for different number of pilot subcarriers for $f_d T = 0.024$.

$$\text{NMSE} \equiv \frac{\text{MSE}}{(f_d T)^2} = \frac{E\{|\widehat{f_d T} - f_d T|^2\}}{(f_d T)^2}. \tag{3.25}$$

Fig. 3.2 compares the NMSE with CRB for different values of M when $P = G = 1$ where the solid curves depict the simulated NMSE results and the dashed curves represent the Cramér-Rao bounds. The maximum normalized Doppler Frequency $f_d T$ is chosen to be 0.024. The number of channel taps (T_d) equals the sample length of the guard interval and the rms delay spread of the channel is $\tau_{rms} = T_d/4$. It is observed that a larger M reduces both the NMSE and CRB. However, the system complexity and the memory required to store $\ln(\det(\boldsymbol{R}))$ and $\boldsymbol{R}^{-1}$ increases proportional to M.

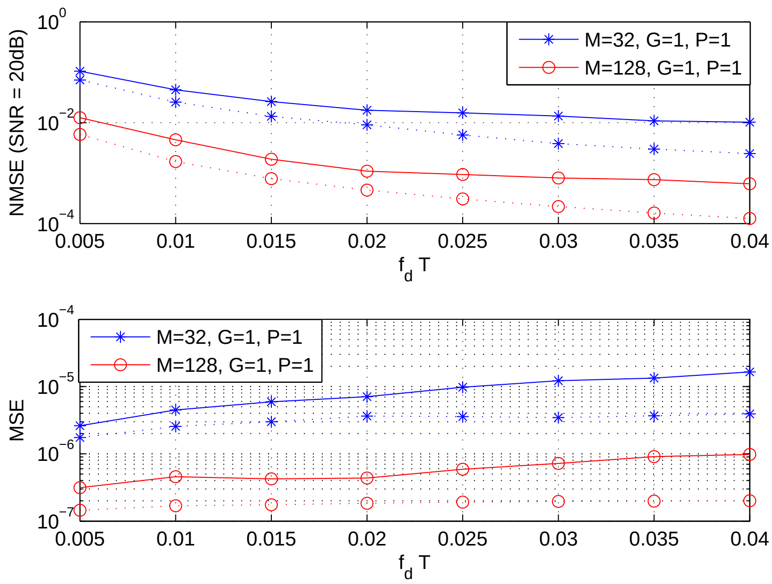

FIGURE 3.4. NMSE and CRB vs. f_dT for SNR = 30dB.

In Fig. 3.3, the NMSE values of the estimator for different values of P, M, and G are depicted when f_dT is set to 0.024. The product $M \times G$ is kept constant to maintain a fixed estimation latency of 28.8 ms. As expected, this figure clearly demonstrates that the system performance improves when more pilot subcarriers per OFDM symbol are used. Employing more than one pilot carriers does not increase the latency since they belong to the same estimation group and the increase in the complexity of the algorithm is negligible.

Fig. 3.4 depicts the performance of the estimator as f_dT changes with different values of M (32 and 128) when $P = 1$, $G = 1$ and the SNR is 20dB. The theoretical CRB lower bound values are also provided. The increase in MSE is expected at higher values of f_dT, however, since the proposed algorithm takes

ICI into account, the performance of the estimator does not deteriorate at higher values of f_dT, as the NMSE reduces when f_dT increases.

We also compare the performance of our scheme with a scheme analogous to [22] and [23], when accurate delay profile information is not available. From now on, we will refer to this method as autocorrelation method or ACM. Considering the number of pilot subcarriers, Q, to be greater or equal to the delay spread T_d, and that there is equal pilot spacing between the pilot subcarriers, a time domain channel estimate can be obtained by applying a Q-point IFFT.

In ACM method, the autocorrelation of the channel estimates and the actual theoretical channel autocorrelation can be compared to obtain an estimate of the maximum Doppler frequency. This can be done using the frequency-domain or time-domain channel estimates. However, the time-domain is applied as in [23], it is suggested that time-domain method outperforms the frequency-domain case. For the ACM method, unlike the proposed method, the channel delay profile needs to be known.

In Fig. 3.5, the NMSE of the ACM is depicted together with the NMSE of the proposed estimator when the delay spread information at the receiver side is incorrect. In this figure, $f_dT = 0.024$, M is set to 128, G is equal to 2 and P is chosen to be 8. T_d represents the delay spread of the channel, while T_d' represents the assumed delay spread at the receiver. As shown in the figure, the proposed method performs better, as the delay spread information is not required.

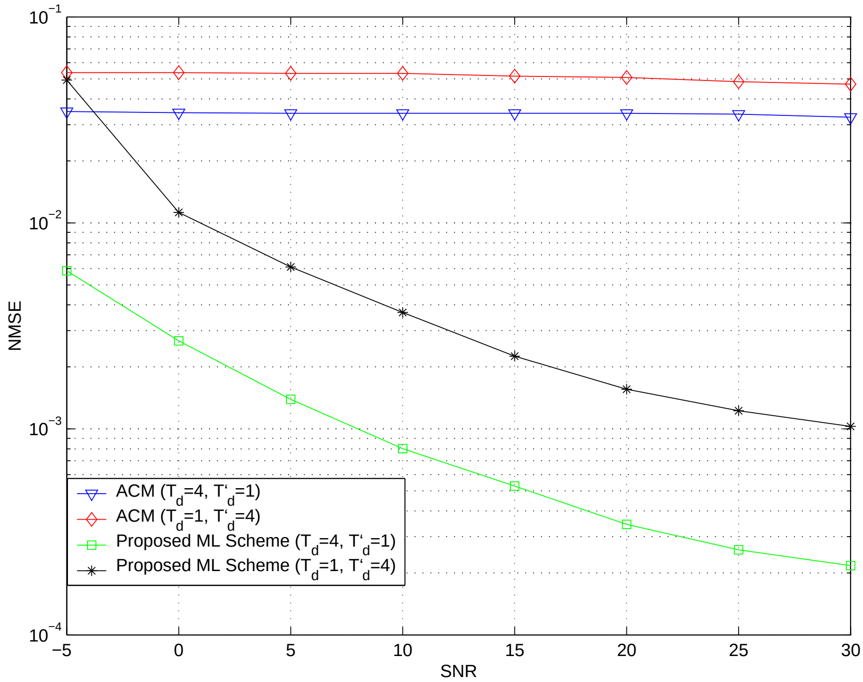

FIGURE 3.5. Performance of ACM and proposed methods when the delay spread information at the receiver is not accurate (T_d: actual channel delay spread, T'_d: erroneous delay spread information at the receiver).

3.4. Conclusion

We have derived an ML algorithm to estimate the maximum Doppler frequency for OFDM systems in time-varying Rayleigh fading channels. The algorithm requires no extra overheads since it employs the already-existing pilot subcarriers. The proposed algorithm takes the effects of ICI into consideration, which results in superior performance even in very fast fading environments. The proposed estimator can be implemented via a filter bank whose coefficients can be stored in the system memory for low-complexity implementation. The estimator works well even when the delay profile information is not available at the receiver side. Many design parameters associated with the proposed algorithm are adjustable to meet various performance requirements. It is shown that the performance can be significantly improved if more pilot carriers from each OFDM symbol is employed. Further improvements in the performance can be obtained at the expense of system complexity by increasing the number of OFDM symbols in one estimation group, or at the expense of latency by summing the cost function over many estimation groups. We have also given the Cramér-Rao bound for the MSE of the Doppler estimates. Simulation results verified the accuracy of the proposed algorithm.

4. PHASE NOISE SUPPRESSION FOR OFDM SYSTEMS OVER FAST TIME-VARYING CHANNELS

4.1. System Description

A doubly-selective channel is considered with a maximum delay of T_d, an rms delay spread of τ_{rms}, and a maximum Doppler frequency f_d. Furthermore, a tapped delay line channel model is adopted with exponentially decaying tap power. The channel coefficient of the l-th tap $(0 \leq l \leq T_d - 1)$ at time n is denoted as $h_l(n)$, and the channel taps are independent identically distributed (i.i.d.), zero-mean, circularly symmetric complex Gaussian random variables. It is further assumed that the autocorrelation of the channel can be modeled by a zeroth-order Bessel function of the first kind [35]. Thus, for the l-th tap at time n, the autocorrelation is expressed as

$$E\left\{h_l(n+\Delta n)h_l^H(n)\right\} = \alpha e^{\frac{-l}{\tau_{rms}}} J_0\left(\frac{2\pi f_d T \Delta n}{N}\right) \tag{4.1}$$

where $(\cdot)^H$ denotes complex conjugate transpose, T is the total duration of N samples, f_d, as mentioned earlier, is the maximum Doppler frequency, $J_0(\cdot)$ represents the zeroth-order Bessel function of the first kind, and α is a scaling factor which is used to normalize the channel power and is given by

$$\alpha = \left(\sum_{l=0}^{T_d-1} e^{\frac{-l}{\tau_{rms}}}\right)^{-1}. \tag{4.2}$$

In this chapter, an OFDM system with N subcarriers is considered. All the subcarriers are assumed to be active. A subset of the subcarriers are reserved for pilot signals used for many purposes such as channel estimation. As commonly adopted, each OFDM symbol is extended by a cyclic prefix of length G, which is not less than the duration of the channel memory (i.e., the maximum delay T_d). This ensures that the received signal is demodulated from channel's steady-state response rather than the transient one. If the received signal is demodulated from the channel's steady-state response, ISI can greatly degrade the system performance.

By defining the data of the k-th subcarrier as d_k, the time-domain signal can be represented as

$$x(n) = \sqrt{\frac{E_s}{N}} \sum_{k=0}^{N-1} d_k e^{j2\pi nk/N}, \quad -G \leq n \leq N-1 \tag{4.3}$$

where E_s is the symbol energy per subcarrier and d_k is the data symbol carried by the k-th subcarrier. The average signal energy is normalized to unity, that is, $E\left\{|d_k|^2\right\} = 1$. This signal then propagates through a time-varying multipath channel, and the received signal can be expressed as

$$y(n) = \sum_{l=0}^{T_d-1} h_l(n)x(n-l). \tag{4.4}$$

After the received signal is down-converted to a lower frequency, typically through a mixer with a local oscillator and some filtering, the effect of phase noise can be modeled by introducing a multiplicative term $\theta(n)$ to the received signal as [36]

$$r(n) = y(n)\theta(n) + \omega(n) \tag{4.5}$$

where $\omega(n)$ is the zero-mean additive white Gaussian noise (AWGN) with variance σ_ω^2 . It is generally accepted that phase noise is dominated by the receiver and the phase noise introduced by the transmitter can be neglected. The basic reasoning for this is the fact that the cost of a local oscillator that does not introduce significant phase noise is much higher. While such a local oscillator can be used at the transmitter side, it might not be feasible for the manufacturers to utilize one at the receiver side, due to cost concerns.

The phase noise process $\phi(n)$ is a time-varying process which is related to the multiplicative disturbance as $\theta(n) = e^{j\phi(n)}$. In the rest of this thesis, the variable $\phi(n)$ will be referred to as "phase noise", and $\theta(n)$ as "phase noise disturbance".

After discarding the cyclic prefix in (4.5), the ISI-free data part of the received signal can be obtained as

$$r(n) = \frac{1}{\sqrt{N}} \sum_{m=0}^{N-1} d_m e^{j2\pi nm/N} e^{j\phi(n)} H_m(n) + \omega(n) \tag{4.6}$$

where

$$H_m(n) = \sum_{l=0}^{T_d-1} h_l(n) e^{-j2\pi lm/N}.$$

From (4.6), the signal on the k-th subcarrier can be expressed as

$$\begin{aligned} R_k &= \frac{1}{\sqrt{N}} \sum_{n=0}^{N-1} r(n) e^{-j2\pi kn/N} \\ &= d_k \frac{1}{N} \sum_{n=0}^{N-1} H_k(n) e^{j\phi(n)} + \alpha_k + W_k \end{aligned} \tag{4.7}$$

where the second and the third term represent, respectively, the ICI and noise components, and are expressed as

$$\alpha_k = \frac{1}{N} \sum_{m=0, m\neq k}^{N-1} d_m \sum_{n=0}^{N-1} H_m(n) e^{j\phi(n)} e^{j2\pi(m-k)n/N} \tag{4.8}$$

$$W_k = \frac{1}{\sqrt{N}} \sum_{n=0}^{N-1} \omega(n) e^{-j2\pi kn/N}. \tag{4.9}$$

Note that the ICI term has two originating factors: the time-varying fading and the phase noise. In most of the previous work, the channel is considered to be time-invariant or quasi-static, i.e., $H_k(n)$, $n = 0, 1, \cdots, N-1$, is the same for each sample in one symbol; thus allowing to be simply denoted as H_k. This assumption greatly simplifies the effect of phase noise and hence its suppression.

If such an assumption is made, the first term of Eq. (4.7) becomes H_k times the common phase error (CPE), which can be denoted as $\frac{1}{N}\sum_{n=0}^{N-1} e^{j\phi(n)}$ [31]. However, for fast time-varying channels with a high normalized maximum Doppler frequency ($f_d T$), such an approximation becomes unrealistic and it is impossible separate the *common* phase error term, as such a term does not exist. Thus, suppression algorithms assuming a quasi-static channel are expected to suffer from a significant performance degradation if the channel cannot be assumed as such. Hence, for fast time-varying channels, a more appropriate algorithm is needed to suppress the phase noise.

In this thesis, a frequency-domain approach is employed which exploits the pilot subcarriers. Consider the pilot subcarriers to belong to a set $\mathcal{K}$. For clarity and simplicity of notation, if a certain subcarrier k is a member of $\mathcal{K}$, the data carried on this subcarrier will be referred to as p_k, instead of d_k. The estimate of the channel for the k-th pilot (p_k) can be obtained as

$$\tilde{H}_k = \frac{1}{N}\sum_{n=0}^{N-1} H_k(n) e^{j\phi(n)} + p_k^{-1}\left(\alpha_k + W_k\right). \tag{4.10}$$

Because of the doubly-selective characteristics of the channel, phase noise estimation for each time instant n becomes extremely complex, if not impossible, even if the channel state information is available. To make the estimation and suppression of the phase noise tractable, a simplified, yet accurate model of the system given in Eq. (4.10) is required. The phase noise process can thus be considered to be quasi-static, i.e., the phase noise to be constant over each OFDM symbol and changes from symbol to symbol. With this simplification, (4.10) can be rewritten as

$$\tilde{H}_k = \frac{e^{j\phi}}{N}\left(\sum_{n=0}^{N-1} H_k(n)\right) + W_k +$$

$$\frac{e^{j\phi}}{N}\left(\sum_{m=0,m\neq n}^{N-1} d_m \sum_{n=0}^{N-1} H_m(n)e^{j2\pi(m-k)n/N}\right) \tag{4.11}$$

where the phase noise disturbance $e^{j\phi}$ is the same for all subcarriers in a specific OFDM symbol, which is considered to be equal to $e^{j\phi(N/2+1)}$. Without loss of generality, the pilot symbols are assumed to be equal to unity. In the next section, the accuracy of the above approximation will be justified with different types of local oscillators and provide the range over which such an approximation is valid.

4.2. Phase Noise Characterization

In this section, the accuracy of the approximation made in (4.11) is justified for both phase-locked and free-running local oscillators. Let us define the mean-square error of the phase noise process due to the quasi-static approximation, as a function of time index n, as

$$e_{\text{MS}}(n) \equiv E\left\{|(\theta(N/2+1)-\theta(n))|^2\right\}. \tag{4.12}$$

4.2.1. Phase-Locked Oscillators

For phase-locked oscillators, $\theta(n)$ can be approximated as $\theta(n) \approx 1 + j\phi(n)$ since $\phi(n) \ll 1$ [32]. The autocorrelation function of $\theta(n)$ is obtained as $R_\theta = 1 + R_\phi$, since $\phi(n)$ is real, zero-mean and stationary. To calculate R_ϕ, one can make use of the power spectral density (PSD) function of the phase noise process. Following the work in [29] (one other PSD function is provided in [28]), the following expression can be obtained

$$\begin{aligned} P_\phi(f) &= 10^{-c} + 10^{-a}, & |f| \le f_1 \\ &= 10^{-c} + 10^{-(f-f_1)\frac{b}{f_2-f_1}-a}, & f > f_1 \\ &= 10^{-c} + 10^{(f+f_1)\frac{b}{f_2-f_1}-a}, & f < -f_1 \end{aligned} \tag{4.13}$$

where $a = 6.5, b = 4, c = 10.5, f_1 = 1$ KHz and $f_2 = 10$ KHz are a typical set of parameters. The parameter c defines the error floor, and a and f_1 are the characteristics of the phase-locked oscillator. The autocorrelation function of ϕ is obtained by taking the inverse Fourier transform of the PSD, by taking into account the sampling frequency.

With the approximation $\theta(n) \approx 1 + j\phi(n)$ and noting that $\phi(n)$ is zero-mean, real, and stationary [29], (4.12) can be rewritten as

$$\begin{aligned} e_{\mathrm{MS}}(n) &= E\left\{(\phi(N/2+1) - \phi(n))^2\right\} \\ &= E\left\{\phi^2(N/2+1)\right\} \\ &\quad - 2E\left\{\phi(N/2+1)\phi(n)\right\} + E\left\{\phi^2(n)\right\} \end{aligned} \tag{4.14}$$

where $E\{\phi^2(N/2+1)\}$ and $E\{\phi^2(n)\}$ are simply equal to the variance of ϕ, and $E\{\phi(N/2+1)\phi(n)\}$ is the autocorrelation function of ϕ.

The normalized mean-square error is further defined as $e_{\mathrm{MS}}(n)/\sigma_\phi^2$, which is expressed as

$$\begin{gathered} e_{\mathrm{NMS}}(n) = 2 - 2R_\phi(n - N/2+1))/\sigma_\phi^2 \\ n = 0, 1, \cdots, N-1. \end{gathered} \tag{4.15}$$

With $a = 6.5$ in (4.13), the average normalized error over one OFDM symbol is obtained to be 8.8×10^{-4}, if $T = 10\mu s$, and 3.5×10^{-3}, if $T = 20\mu s$. If a is selected to be 1, the corresponding error values are similar to those obtained for $a = 6.5$. The normalized error as a consequence of approximating $\phi(n)$ as a quasi-static process, increases proportional to the duration of the OFDM symbol; an OFDM symbol shorter than $50\mu s$ will have negligible error which would allow us to use (4.11) for accurate phase noise estimation and suppression.

4.2.2. Free-Running Oscillators

Let us denote the carrier frequency as f_c, and the actual frequency seen by the receiver is $f_c + f_{\mathrm{dev}}$, where f_{dev} is the deviation from f_c and is assumed to be a zero-mean, white Gaussian process. The process $\phi(t)$ in the free-running case is obtained by integrating $f_{\text{dev}}(t)$ as $\int_0^t f_{\text{dev}}(t)dt$ and is modeled as a nonstationary Wiener process with infinite power [36]. In order to obtain the autocorrelation of the phase-noise disturbance, $\theta(t)$, which is assumed to be stationary, one can continue to work in the continuous-time domain. The autocorrelation of $\theta(t)$ can be defined as $R_\theta(t_1, t_2) = E\{\theta(t_1)\theta^*(t_2)\}$ ($(\cdot)^*$ denotes complex conjugate), which can be written as a function of f_{dev} as

$$\begin{aligned} R_\theta(t_1, t_2) &= E\left\{e^{j(\phi(t_1)-\phi(t_2))}\right\} \\ &= E\left\{e^{j\int_{t_2}^{t_1} f_{\text{dev}}(u)du}\right\} \end{aligned} \tag{4.16}$$

where $\int_{t_2}^{t_1} f_{\text{dev}}(u)du$ is a Gaussian process with variance $2\pi\beta|t_1 - t_2|$ [26] and β represents the two-sided, 3-dB bandwidth of the Lorentzian PSD of the free-running oscillator. For the simplicity of expression, from now on the zero-mean Gaussian variable $\int_{t_2}^{t_1} f_{\text{dev}}(u)du$ will be referred to as α (zero-mean and with variance $\sigma_\alpha^2 = 2\pi\beta|t_1 - t_2|$), and Eq. 4.16 can be expressed as

$$\begin{aligned} R_\theta(t_1, t_2) &= E\left\{e^{j\alpha}\right\} \\ &= \frac{1}{\sqrt{2\pi\sigma_\alpha^2}} \int_{-\infty}^{\infty} e^{j\alpha} e^{-\frac{1}{2}\left(\frac{\alpha}{\sigma_\alpha}\right)^2} d\alpha \end{aligned} \tag{4.17}$$

For any Gaussian random variable with zero-mean, the characteristic function can be expressed as in the following equation [37].

$$\begin{aligned} \mathbf{\Phi}(\omega) &= \frac{1}{\sqrt{2\pi\sigma_\alpha^2}} \int_{-\infty}^{\infty} e^{j\omega\alpha} e^{-\frac{1}{2}\left(\frac{\alpha}{\sigma_\alpha}\right)^2} d\alpha \\ &= e^{-\sigma^2\omega^2/2} \end{aligned} \tag{4.18}$$

Using Eq.4.18 it can be shown that the expression in Eq. 4.17 equals $\mathbf{\Phi}(1)$ and can be written as:

$$E\left\{e^{j\alpha}\right\} = \mathbf{\Phi}(1) = e^{-\sigma_\alpha^2/2} \tag{4.19}$$

The autocorrelation function can then be obtained using Eq. 4.19 as

$$R_\theta(t_1, t_2) = e^{-\pi\beta|t_1 - t_2|} = e^{-\pi\beta\Delta t} \tag{4.20}$$

where $R_\theta(t_1, t_2)$ is dependent only on the time difference since the process θ is assumed to be stationary.

Since the PSD of free-running oscillators obeys the Lorentzian/Cauchy distribution, the Fourier transform of (4.20) should give us the Lorentzian distribution. This can be easily verified as the above function is the characteristic function (i.e., the inverse Fourier transform) of a zero-median Lorentzian distribution.

The mean-square error given in (4.12) for the case of free-running oscillators can now be expressed as

$$\begin{aligned} e_{\text{MS}}(n) = E\left\{|\theta(N/2+1)|^2\right\} + E\left\{|\theta(n)|^2\right\} - \\ E\left\{\theta(n)\theta^*(N/2+1)\right\} - E\left\{\theta(N/2+1)\theta^*(n)\right\} \end{aligned} \tag{4.21}$$

where $E\left\{|\theta(N/2+1)|^2\right\}$ and $E\left\{|\theta(n)|^2\right\}$ are equal to the variance of θ, and the two remaining terms are equal to $R_\theta(|N/2+1-k|)$. With the normalized mean-square error given in (4.15), one can rewrite (4.21) as

$$e_{\text{NMS}}(n) = 2 - 2e^{-\pi\beta|N/2+1-n|}/\sigma_\theta^2. \tag{4.22}$$

By quantitatively evaluating the above expression, the range over which (4.11) is valid can be determined for any specific value of β. As suggested in [38], the variance of ϕ for one OFDM symbol ($2\pi\beta T$) is expected to be much less than 1. For σ_ϕ^2 values of 10^{-4} and 10^{-3}, average normalized mean-square error values of 2.4 10^{-4} and 2.5 10^{-3} are observed, respectively. When the values of σ_ϕ^2 are below 10^{-2}, (4.11) can be considered to be valid.

4.3. Maximum Likelihood Scheme For Phase Noise Suppression

The proposed phase noise suppression method is an ML approach which exploits the pilot symbols. As shown in the previous section, under almost all practical scenarios, $\tilde{H}_k$ can be calculated using (4.11). Let subscript u represent the index of the u-th OFDM symbol. Estimating ϕ_u, the phase noise process of the u-th OFDM symbol, is not necessary for phase noise suppression; instead, the estimate of the respective phase noise distortion θ_u is sufficient for this purpose.

The proposed approach works as follows. First, the initial phase noise distortion, θ_1, is estimated using the preamble of OFDM symbols. For 802.11a, both the short and the long preambles sent by the transmitter are known to the user, which allows us to correctly estimate θ_1. However, the only information that is available in the data part is the pilot subcarriers in the frequency domain. Once θ_1 is estimated, the column vector $\boldsymbol{H}_u$ can be obtained by vertically stacking $\tilde{H}_{k,u}$ for all pilot subcarriers of the u-th OFDM symbol. Eq. (4.11) can be rewritten as

$$\tilde{H}_{k,u} = \theta_u H_{k,u} + \theta_u \alpha_{k,u} + W_{k,u} \tag{4.23}$$

where $H_{k,u} = \frac{1}{N}\sum_{n=0}^{N-1} H_{k,u}(n)$. Although $\alpha_{k,u}$ is a weighted Gaussian variable, through the central limit theorem, $\tilde{H}_{k,u}$ can be approximated as a zero-mean, circularly symmetric, complex Gaussian random variable.

The cross-correlation function between $\boldsymbol{H}_{u+\Delta u}$ and $\boldsymbol{H}_u$ can be derived as

$$E\{\boldsymbol{H}_{u+\Delta u}\boldsymbol{H}_u^*\} = \boldsymbol{R}_{\Delta u}\left(\theta_{u+\Delta u}\theta_u^{-1}\right) \tag{4.24}$$

where the identity $\theta^* = \theta^{-1}$ is used. From (4.23), $\boldsymbol{R}_{\Delta u}$ can be defined as

$$\boldsymbol{R}_{\Delta u} = \boldsymbol{R}_{\Delta u}^{|H|^2} + \boldsymbol{R}_{\Delta u}^{\alpha H^*} + \boldsymbol{R}_{\Delta u}^{H\alpha^*} + \boldsymbol{R}_{\Delta u}^{|\alpha|^2} + \delta(\Delta u)\sigma_\omega^2 I \tag{4.25}$$

where the correlation matrices $\boldsymbol{R}_{\Delta u}^{|H|^2}$, $\boldsymbol{R}_{\Delta u}^{\alpha H^*}$, $\boldsymbol{R}_{\Delta u}^{H\alpha^*}$, and $\boldsymbol{R}_{\Delta u}^{|\alpha|^2}$ can be found in Chapter 3 and [45] for the same channel model used in this chapter. It is important to note that these correlation matrices do not depend on u, but rather on Δu. Thus, if the channel delay profile and the maximum Doppler frequency are known, these correlation matrices can be conveniently stored in the system memory, which greatly reduces the system complexity and makes it implementable for practical applications.

Next, the vector $\boldsymbol{H}'_u$ is defined as

$$\boldsymbol{H}'_u = [\boldsymbol{H}_{u-1} \quad \boldsymbol{H}_u]^T \tag{4.26}$$

whose correlation matrix $\boldsymbol{R}'_u$ can be obtained as

$$\boldsymbol{R}'_u = \begin{bmatrix} \boldsymbol{R}_0 & \boldsymbol{R}_{-1}\theta_{u-1}\theta_u^{-1} \\ \boldsymbol{R}_1\theta_u\theta_{u-1}^{-1} & \boldsymbol{R}_0 \end{bmatrix}. \tag{4.27}$$

Once $\boldsymbol{R}_{-1}$, $\boldsymbol{R}_0$, and $\boldsymbol{R}_1$ are calculated and the estimate of θ_{u-1} is obtained, parameter θ_u can be estimated using the following cost function

$$\Lambda_u(\theta_u) = \ln(\det(\boldsymbol{R}'_u)) + \tilde{\boldsymbol{H}}_1'^{H} \, [\boldsymbol{R}'_u]^{-1} \, \tilde{\boldsymbol{H}}'_u \tag{4.28}$$

where $\tilde{\boldsymbol{H}}'_u$ is the estimate of $\boldsymbol{H}'_u$. Minimizing this cost function is equivalent to maximizing the log-likelihood function of $\boldsymbol{H}'_u$, which is the logarithm of the complex Gaussian vector pdf, as $\boldsymbol{H}'_u$ can be considered Gaussian. The ML estimate of the phase noise distortion, $\hat{\theta}_u$, can be obtained as

$$\hat{\theta}_u = \arg\min_{\theta}(\Lambda_u(\theta)) \tag{4.29}$$

where the search range for $\theta = e^{j\phi}$ equals $-\pi \leq \phi \leq \pi$. Once $\hat{\theta}_u$ becomes available, the phase noise correction can be easily done by multiplying $\boldsymbol{H}_u$ by $\hat{\theta}_u^{-1}$.

4.4. Simulation Results

In the simulations, the OFDM system is assumed to have 512 subcarriers, and every one out of four subcarriers as a pilot subcarrier. The channel coefficients are generated to obey the autocorrelation function given in (4.1). The guard interval has a length of 4 samples ($G = 4$), which also equals the number of channel taps (T_d). In obtaining the bit-error-rate (BER) curves, 1000 OFDM symbols are used, and one in 500 symbols is designated as the OFDM preamble. Channel estimates for data symbols are obtained by exploiting the pilot subcarrier through interpolation.

In Fig. 4.1, free-running oscillators are considered for βT values of 10^{-2}, 10^{-3}, and 10^{-4}. The search range to determine the ML estimate of the phase noise distortion in this case was from $-\pi$ to π, with a step size of 0.04. The dashed lines correspond to the case with $f_d T = 0.01$, while the solid lines are for the case of $f_d T = 0.04$. The OFDM symbol duration T is chosen to be 100μs; thus, the corresponding values of β (two-sided 3dB bandwidth of the Lorentzian PSD) are 1592, 159.2, and 15.92. The phase noise suppression algorithm proposed in this chapter has comparable performances to the ideal case $-$ phase noise free $-$ even when the channel exhibits very fast fading. The error floor when $f_d T = 0.04$ is due to the severe ICI caused by fast fading. Employing more complex channel estimation and data detection schemes can reduce or eliminate the error floor, which is beyond the scope of this thesis. Furthermore, lowering the value of β increases the performance slightly, which is expected.

In Fig. 4.2, the performance of the algorithm for phase-locked oscillators is provided for $a = 1$ and $T = 20\mu s$. The dashed and solid lines represent the cases with $f_d T = 0.01$ and $f_d T = 0.04$, respectively. Unlike the case of free-

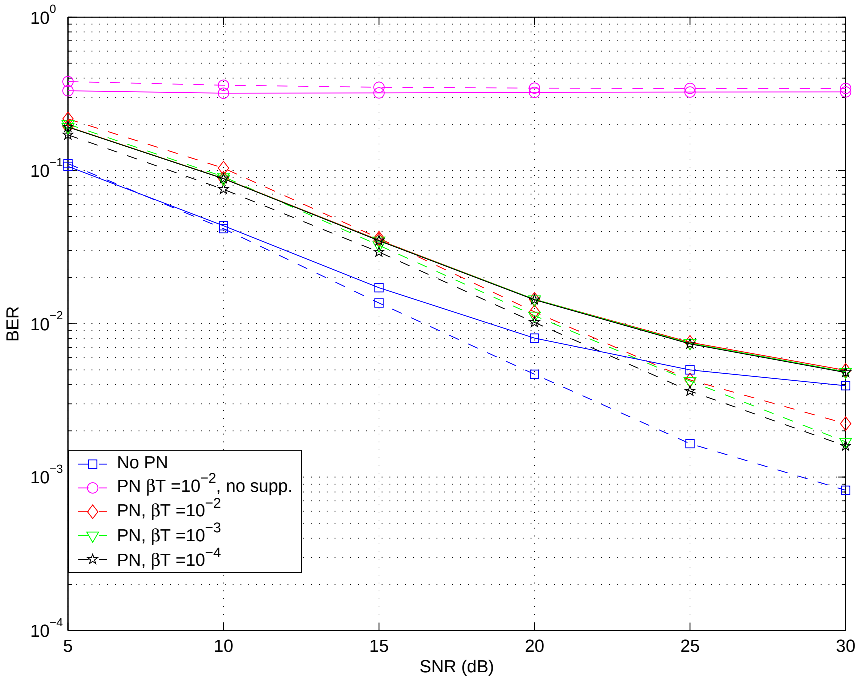

FIGURE 4.1. BER vs. SNR for free-running oscillators ($\beta T = 10^{-2}$, 10^{-3}, and 10^{-4}; dashed lines: $f_d T = 0.01$, solid lines: $f_d T = 0.04$).

running oscillators, the effect of the phase noise on the system performance is much milder in this case. The algorithm presented in this chapter still increases the performance of the system, but the improvement is less than the free-running case.

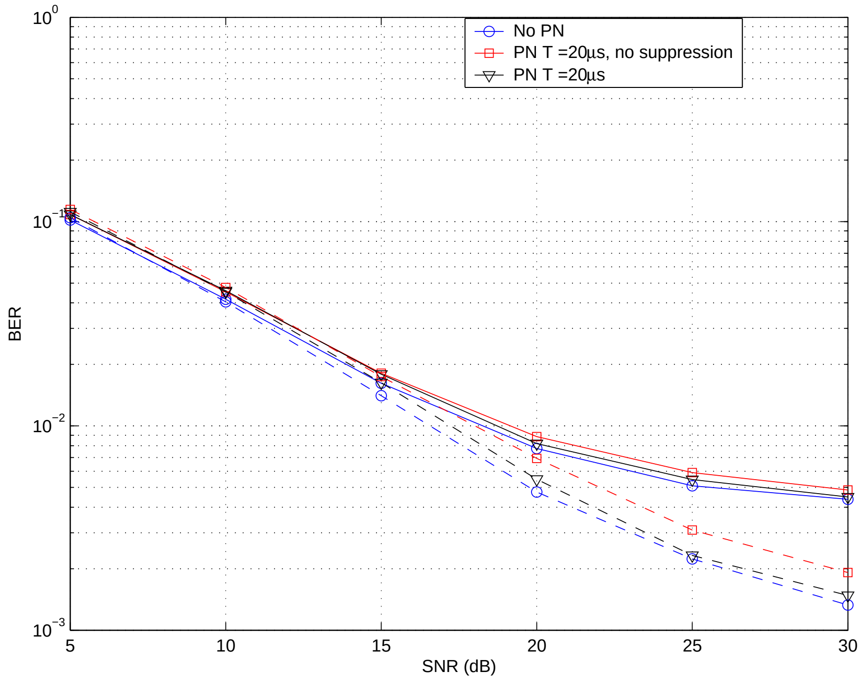

FIGURE 4.2. BER vs. SNR for phase-locked oscillators ($T = 20\mu s$, $a = 1$; dashed lines: $f_dT = 0.01$, solid lines: $f_dT = 0.04$).

4.5. Conclusion

In this chapter, an algorithm to suppress phase noise for OFDM systems over doubly-selective channels is developed, especially those with a high normalized maximum Doppler frequency, for which a quasi-static fading model is unacceptable and a simple common phase error (CPE) term does not exist. This method is applicable to both phase-locked and free-running local oscillators. The algorithm is a maximum likelihood approach that exploits the pilot subcarriers, whose coefficients can be stored in the system memory to reduce the complexity. With typical sets of system and channel parameters, the performance improvement due to phase noise suppression is found to be more significant for the case with free-running oscillators than with phase-locked oscillators.

5. MOBILE DIRECTION ASSISTED PREDICTIVE BASE STATION SWITCHING FOR BROADBAND WIRELESS SYSTEMS

5.1. Predictive Base Station Switching

Broadband wireless systems such as those designed according to the IEEE 802.16e standard are expected to support hard handover (HHO), fast base station switching (FBSS), and soft handover or macro diversity handover (MDHO) schemes. In FBSS, the MS transmits to and receives from only one BS called the *anchor* BS, which is similar to HHO; however, a faster method to perform handover operations is provided. In MDHO, the MS can transmit to/receive from one or more BSs. The initial-ranging/handover-ranging codes are also provided in the IEEE 802.16e standard to ensure that the MS can sort the BSs based on their signal strength.

In the proposed PBSS, the selection of the new serving/anchor BS is based on the current direction and the speed of the mobile. The target/diversity-list BSs are selected via the MS direction information, and in case the signal level from the serving/anchor BS drops below a certain level, a step to *predict* the future behavior of the MS is introduced. In this prediction step, a decision metric λ_{BS} is calculated for each BS. This decision metric is the ratio of the expected time period that the MS will be connected to a certain BS, P_{BS}, and the average MS-BS distance while it is connected to a certain BS, $\overline{d}_{\mathrm{BS}}$. The minimum length of the prediction step is proportional to the speed of the MS and it does not end until the MS exits the effective range of each neighboring/diversity-list BS.

To avoid ping-pong effects and to ensure seamless handover, two signal threshold levels defining the effective and maximum ranges of a certain BS are employed. The first threshold, T_1, is employed to define the effective BS range

R_{BS}, and to decide whether a handover is required. If the signal level obtained from the handover-ranging codes is below T_1, the prediction step starts and decision metrics for each neighboring/diversity-list BS are obtained. The second threshold, T_2, defines the maximum range of a certain BS. Even if a BS has the highest decision metric, it is not selected as the new serving/anchor BS if the MS will be outside the maximum range of the serving/anchor BS at the time of handover.

As mentioned earlier, direction and speed information of the MS are used in PBSS. The speed information can be obtained using the estimated maximum doppler frequency as in [45]. However, this method might not be employed to estimate the direction of the MS. If the MS is equipped with GPS, the MS should continuously notify the anchor/serving BS of its coordinates. On the other hand, if the MS is provided with the exact coordinates of the neighboring/diversity-list BSs, the MS can also help in the decision process of selecting its new serving/anchor BS. This will distribute the handover decision-making process among the network and the mobile stations. Since GPS is based on the information from the satellites, it will not properly operate in dense urban areas or in indoor environments. In this case, other location-estimation schemes such as those based on propagation delay times [46], path loss, angles of arrival and power delay profile [47], [48] could be employed. Once the location information is available, by taking samples at different time instants, necessary speed and direction information can be obtained. While the estimation of the speed and direction of the MS is out of the scope of this work, it is shown that even when the direction information is not precise, PBSS still outperforms classical approaches that are based only on the signal levels and the current distance to the serving BS.

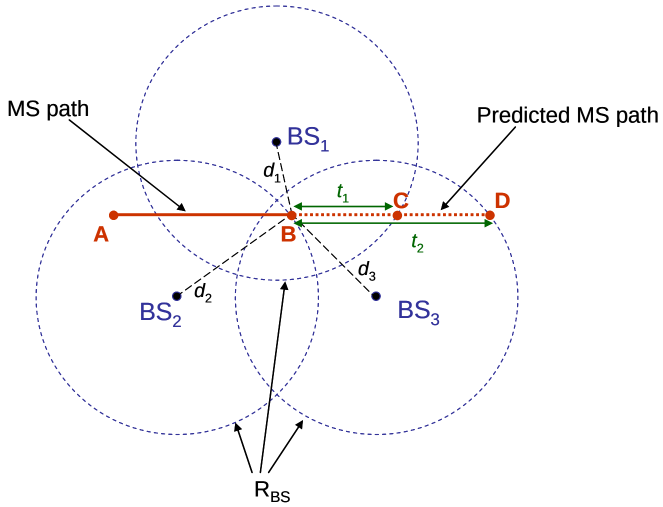

FIGURE 5.1. An example of a handover scenario where $d_1 > d_3 > d_2$ and $t_2 > t_1$.

To better explain our motivation, let us consider a hard handover case for the scenario shown in Fig. 5.1. Suppose that initially the MS is at point **A** and the serving BS is BS_2. After a certain time, it will arrive at point **B**. Under normal fading and shadowing conditions, the signal level measured using handover-ranging codes will likely to be less than T_1, and it will thus enter the hysteresis mode. A classical algorithm making use of only the signal level and current distance to the serving BS will likely choose BS_1 as the new serving BS if there are no significant shadowing effects. When the MS arrives at point **C**, it will be in hysteresis again and it will need to switch to another BS, which is most likely to be BS_3. However, at point **B**, the MS was already in R_{BS_3}. The main aim of the proposed algorithm is to avoid the unnecessary handover to BS_1. Of course, under some extreme fading and shadowing conditions, it might be needed to handover to BS_1; but this is in general not absolutely necessary.

The decision metric λ_{BS} is obtained by predicting the future behavior of the MS, which is shown by dotted lines in Fig. 5.1. Naturally, the decision metric is proportional to P_{BS}, as selecting the BS that ensures a longer connection will reduce the number of handovers. However, if there are two BSs with comparable P_{BS} values, it is preferable to pick the one that would ensure a higher expected signal level, and hence a smaller $\overline{d}_{\mathrm{BS}}$ value. If the MS were to completely cross the effective range of all BSs in the target/diversity BS list during the prediction step, then either P_{BS} or $1/\overline{d}_{\mathrm{BS}}$ could have been interchangeably used as the decision metric. For the scenario shown in Fig. 5.1, the time spent in BS_1 is t_1 and the time spent in BS_3 is t_2, where $t_2 > t_1$. Since the average distance of the MS to BS_1 from point **B** to **C** and to BS_3 from point **B** to **D** are comparable, the decision metric of the proposed algorithm would suggest a handover to BS_3, instead of BS_1 at point **B**.

The flow chart of the proposed algorithm is shown in Fig. 5.2, where BS_0 is the current serving/anchor BS. Many handover algorithms are composed of a detection step where a decision metric is checked to see whether a handover decision is required, and a decision step where the handover is executed. In the proposed PBSS algorithm, after the decision step, there is a prediction step where the decision metrics of the neighboring/diversity-list BSs are calculated. The final step is the execution step where a handover to the *optimum* BS based on the decision metrics is performed. The prediction step in PBSS ensures a lower average number of handovers without degrading the signal level as it will be shown in the simulation results section.

As depicted in Fig. 5.2, if a handover decision has been made, there will not be a new prediction step until that handover decision is executed or unless the direction of the MS changes before the handover execution step. The BS with the

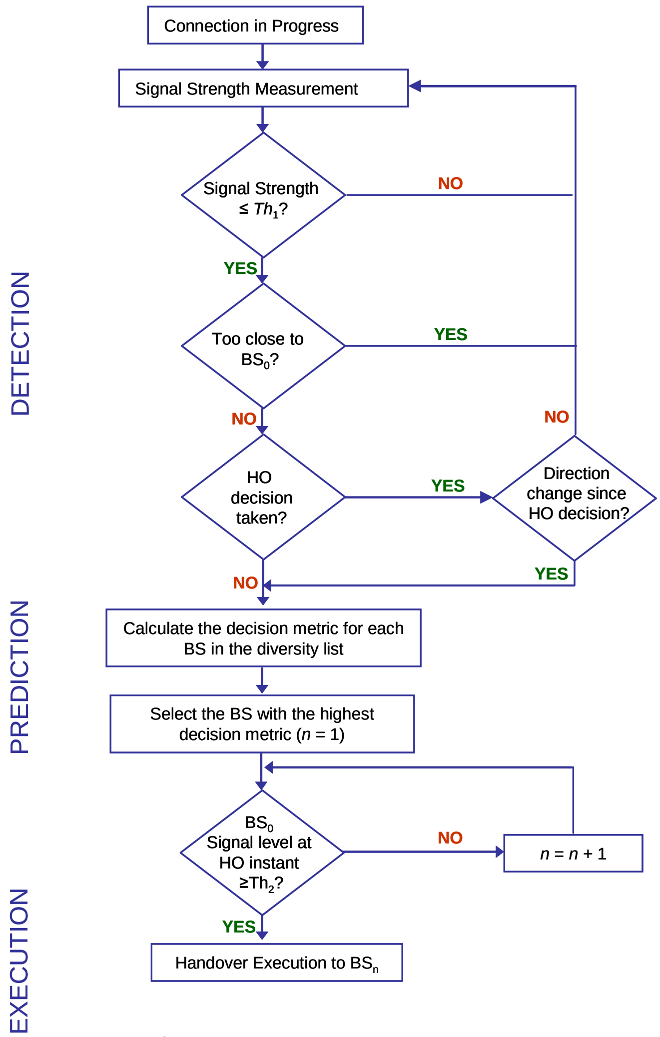

FIGURE 5.2. Flow chart of the proposed predictive base station switching algorithm.

highest decision metric will not automatically become the next serving/anchor BS as the expected signal level of the MS at the time of handover should be greater than T_2 for a handover to take place. If this is not the case, then the BS with the next highest decision metric is checked.

The proposed algorithm has a low complexity and requires little message overhead. The calculation of the critical parameter $\overline{d}_{\mathrm{BS}}$, as will be shown in the next section, requires only the MS speed and the time instants at which the MS enters and leaves the effective range of the BS, R_{BS}.

5.2. Calculation of The Average MS-BS Distance

Calculation of the average MS-BS distance, $\overline{d}_{\mathrm{BS}}$, is an important part of the PBSS algorithm. To illustrate how this calculation is performed, Fig. 5.3 can be used. Since the MS speed and direction are considered to be known, the time spent in the R_{BS}, t_{BS}, is also known. This information can be accurately obtained by performing prediction in the reverse MS direction until the MS exits R_{BS}, since the speed of the MS might have been changed after it had entered R_{BS}.

T is considered to be the sampling period and that there are N sample points spent in R_{BS}. d_P is defined as the line along the trajectory of the MS ($d_P = v_{\mathrm{MS}} t_{\mathrm{BS}}$, where v_{MS} is the MS speed.) and $d_\perp$ as the line that perpendicularly crosses d_{P}. At each prediction step i, the distance of the MS to the BS, d_i, $d_\perp$, and the line from the current MS location to the intersection point of d_P and $d_\perp$ (i.e., $\mid d_P/2 - v_{\mathrm{MS}}(i-1)T \mid$) form a perpendicular triangle. Using this information, the following equations can be written:

$$\sin(\alpha_i) = \frac{d_\perp}{d_i} \tag{5.1}$$

$$\cos(\alpha_i) = \frac{\mid d_P/2 - v_{\mathrm{MS}}(i-1)T \mid}{d_i} \tag{5.2}$$

Using the trigonometric equality $\cos^2(\alpha_i) + \sin^2(\alpha_i) = 1$ and Eqs. 5.1 and 5.2, the following expression can be obtained

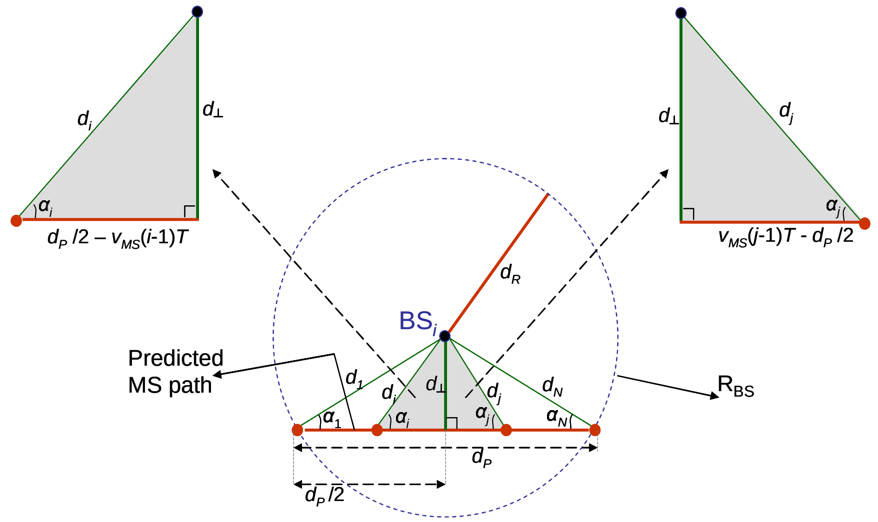

FIGURE 5.3. Calculation of the average BS-MS distance.

$$d_i^2 = d_\perp^2 + \frac{d_P^2}{4} + v_{\text{MS}}^2[(i-1)T]^2 - d_P v_{\text{MS}}(i-1)T. \tag{5.3}$$

Furthermore, considering d_{R} to denote the radius of the effective cell of a certain BS, Eq. 5.4 can be written.

$$d_\perp^2 = d_{\text{R}}^2 - \frac{v_{\text{MS}}^2[(N-1)T]^2}{4} \tag{5.4}$$

Substituting Eq. (5.4) into Eq. (5.3) and considering $d_P = v_{\text{MS}} t_{\text{BS}} = v_{\text{MS}}(N-1)T$, one can obtain

$$d_i^2 = d_{\text{R}}^2 - \frac{v_{\text{MS}}^2[(N-1)T]^2}{4} + \frac{v_{\text{MS}}^2[(N-1)T]^2}{4} + v_{\text{MS}}^2[(i-1)T]^2 - v_{\text{MS}}^2(i-1)(N-1)T^2. \tag{5.5}$$

By rearranging Eq. (5.5), the following equation can be derived.

$$d_i = \sqrt{d_{\text{R}}^2 + v_{\text{MS}}^2 T^2 (i-1)(i-N)}. \tag{5.6}$$

In Eq. (5.6), the radius of the R_{BS} and MS speed information when the prediction step starts are required. If these are available, the average distance can be calculated as

$$\begin{aligned}\bar{d}_{\mathrm{BS}} &= \frac{1}{N}\sum_{i=n_e}^{N} d_i \\ &= \frac{1}{N}\sum_{i=n_e}^{N} \sqrt{d_{\mathrm{R}}^2 + v_{\mathrm{MS}}^2 T^2 (i-1)(i-N)}\end{aligned} \tag{5.7}$$

where n_e is the effective sampling instant to start the averaging. If the MS enters R_{BS} during the prediction step, then this value is 1. Otherwise (as in the scenario in Fig. 5.1), this information can be obtained as t_{BS} and P_{BS} are known.

5.3. Calculation of Cell Outage Probability

In this section, the cell outage probability of the PBSS algorithm is derived, and the results are compared with a classic BS switching (CBSS) algorithm. From the point of view of the flow chart in Fig. 5.2, CBSS has a similar detection method (except that the changes in direction are not monitored), which is followed directly by the execution step. Before calculating the cell outage probability based on path loss and shadowing effects, the outage probability of the system at a certain distance from the BS has to be defined. The outage probability at r $(0 \leq r \leq R)$ is defined as the probability that the received power is less than a predetermined threshold, $\boldsymbol{P}_{\mathrm{th}}$ as presented in the next equation.

$$P_{\mathrm{out}}(\boldsymbol{P}_{\mathrm{th}}, r) = P\{\boldsymbol{P}(r) < \boldsymbol{P}_{\mathrm{th}}\} \tag{5.8}$$

To be able to define the received power, the log-normally distributed shadowing and simplified path loss models presented in [8] can be used. The received power in dB can then be expressed as:

$$\boldsymbol{P}_r = \boldsymbol{P}_t + 10\log_{10} K - 10n\log_{10}\left(\frac{r}{r_0}\right) - \upsilon \tag{5.9}$$

where n is the path loss exponent, K is a the known/measured value at distance r_0, and υ, representing the shadowing effect in dB, is a Gaussian distributed random variable with zero-mean and a variance of σ_υ^2. Using this equation, and considering υ is a zero-mean Gaussian random variable, $P_{\text{out}}(\boldsymbol{P}_{\text{th}}, r)$ can be written as follows

$$P_{\text{out}}(\boldsymbol{P}_{\text{th}}, r) = 1 - Q\left[\frac{\boldsymbol{P}_{\text{th}} - \left(\boldsymbol{P}_t + 10\log_{10} K - 10n\log_{10}\left(\frac{r}{r_0}\right)\right)}{\sigma_\upsilon}\right] \tag{5.10}$$

.

Using $P_{\text{out}}(\boldsymbol{P}_{\text{th}}, r)$, the ratio of the area within the cell that meets or exceeds the minimum power requirement can be expressed as, P^C, which can be defined as:

$$P^C = \frac{1}{\pi R^2}\int_0^{2\pi}\int_0^R \left(1 - P_{\text{out}}(\boldsymbol{P}_{\text{th}}, r)\right) r dr d\theta. \tag{5.11}$$

Using Eq. 5.11, the cell outage probability P_{out}^C, can be defined as the ratio of area of the cell that does not meet the minimum power requirements to the total area of the cell, and can be represented as

$$\begin{aligned} P_{\text{out}}^C(R) &= 1 - P^C \\ &= 1 - \frac{1}{\pi R^2}\int_0^{2\pi}\int_0^R \left(1 - P_{\text{out}}(\boldsymbol{P}_{\text{th}}, r)\right) r dr d\theta \end{aligned} \tag{5.12}$$

.

In Eq. 5.12, it is considered that all the MS in the cell area are uniformly distributed. Although it might be reasonable to consider a uniform distribution over the azimuth angle, θ; the distribution along the radius r (with a probability density function (pdf) of $P_r(r)$), might not be uniform. To obtain the pdf of the users in the total cell area, we can use the following equation

$$P(r) = \frac{P_r(r)}{\int_0^R 2\pi P_r(r) r dr}. \tag{5.13}$$

If a uniform distribution along r is considered, then $P(r) = \frac{1}{\pi R^2}$ is obtained, which is considered in Eq. 5.11. It is important to note that, Eq. 5.12 considers that the MS-BS distances are distributed uniformly over the cell area. Although both CBSS and PBSS use the same cell structure, their cell outage probability is not exactly the same, as on the average, PBSS might have a higher relative MS-BS distance. To be able to calculate the cell outage probability for these two schemes, let's consider the pdf of the location of the users of PBSS over r to be $P_r(r) = P_{PBSS}(r)$, and similarly that of CBSS as $P_r(r) = P_{CBSS}(r)$.

Using Eq. 5.12 and Eq. 5.13, the cell outage probability specifically designed to show the difference between PBSS and CBSS schemes can be defined to be ($P_{\text{out}}^{\text{PBSS}}$ and $P_{\text{out}}^{\text{CBSS}}$, respectively) as

$$P_{\text{out}}^{\text{PBSS}} = 1 - \int_0^{2\pi} \int_0^R P_{PBSS}(r) \left(1 - P_{\text{out}}(\boldsymbol{P}_{\text{th}}, r)\right) r dr d\theta \tag{5.14}$$

$$P_{\text{out}}^{\text{CBSS}} = 1 - \int_0^{2\pi} \int_0^R P_{CBSS}(r) \left(1 - P_{\text{out}}(\boldsymbol{P}_{\text{th}}, r)\right) r dr d\theta \tag{5.15}$$

Note that evaluating the above equations analytically might be troublesome. However, these equations can be evaluated numerically to obtain the outage probability for CBSS and PBSS as shown in section 5.4.

5.4. Simulation Results

For the simulations, a hexagonal cell configuration is considered. In the IEEE 802.16e standard, the BER target is set to be 10^{-6} and for QPSK-1/2 the required minimum received power is -90 dBm when all the subchannels are utilized. It is further assumed that the maximum MS power is 1 watt, or 30 dBm; thus, the maximum path loss including tolerance to shadowing effect is 120 dB. The MS-BS distance is determined to be 500 m using the path loss model. We consider a total of 100 BSs. The speed of each MS in the simulation is different, ranging from 0 m/s to 16 m/s or about 57 km/h, which is specifically chosen as the IEEE 802.16e standard is expected to provide mobility up to 60Km/h. The MS directions along the x-axis and y-axis are assumed independent and can change at any instant. Since the algorithm is based on the direction information, the performance of PBSS is evaluated for various probabilities of direction change at any given instant, ranging from $P_{\text{dir}} = 0$ to $P_{\text{dir}} = 0.2$. Both x and y direction values, d_x and d_y, can be -1, 0, or 1. When $d_x = 0$ and $d_y = 0$, the MS is considered stationary. We adopt the simple path loss model given in [8] and include the lognormal distributed shadowing effects. The model related parameters are: the path loss exponent is 3.5, the path loss intercept (path loss at 1 km) is 125 dB, and the shadowing standard deviation is 8 dB.

Although an average shadowing condition is used in the modeling of PBSS (in which case the effective cell boundary becomes a circle whose radius is determined by the path loss), random shadowing effects, which cause the cell shape to become irregular, are considered in the simulations. The result of these simulations show the effectiveness of PBSS in practical situations.

The performance of PBSS is compared with that of a classic BS switching (CBSS) algorithm, where if the signal level is less than T_1 and if the MS is not too close to the serving/anchor BS, a handover is performed to the BS that has the strongest signal level. If the MS is close to the serving/anchor BS, but the signal level is less than T_2, a handover is also executed. Basically, CBSS has a similar detection method as shown in Fig. 5.2, except that changes in direction are not monitored. The detection is followed directly by the execution step.

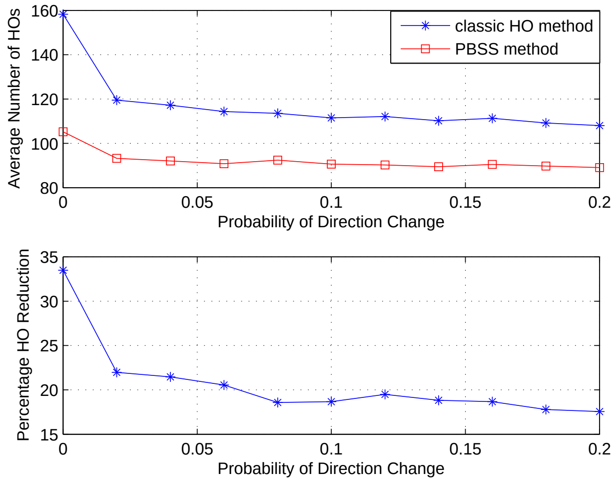

FIGURE 5.4. Average number of handovers and the percentage handover reduction by PBSS versus P_{dir}.

Fig. 5.4 shows the average number of handovers versus the percentage of handover reduction due to the use of PBSS with respect to P_{dir}. The handover values are averaged over 1000 MSs for 4000 seconds. It is observed that the performance improvement is always above 17%. As expected, the greatest improvement of 33.5% occurs when the MS does not change its traveling direction.

Note that the number of handovers decreases when the value of P_{dir} increases from zero, or in other words, when the trajectory of the MS changes from fixed to random. This is intuitively simple to understand: if the speed and direction of the MS do not change, the minimum number of handovers occurs only when the MS travels along a line that crosses multiple BS locations. Otherwise, the number of handovers is expected to be high as can be seen from Fig. 5.1. When the MS moves at random directions (large P_{dir} values), it has a higher probability compared to the case of $P_{\mathrm{dir}} = 0$ to stay in the same cell area within a given amount of time. The effect of P_{dir} becomes less significant once the MS starts to move in a random manner.

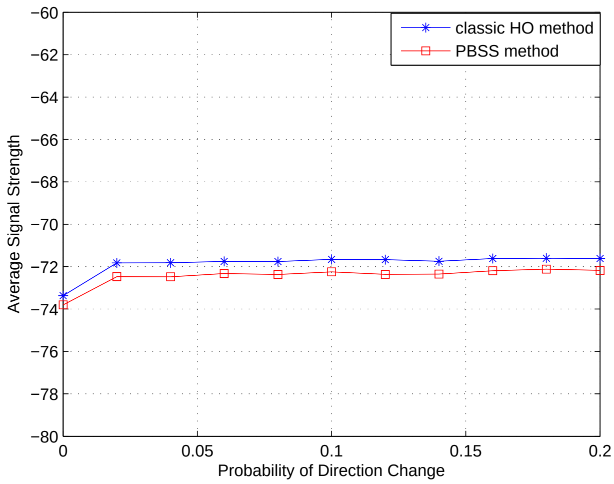

FIGURE 5.5. Average signal strength (dBm) of CBSS and PBSS with versus P_{dir}.

Fig. 5.5 shows the received signal levels at the BS versus P_{dir}. It is observed that the difference between the signal levels with CBSS and the proposed PBSS for all values of P_{dir} is within about half a dB. Considering the inherent advantages of PBSS in reducing the handover delay and in lowering signaling overhead and network resources, it could be a more attractive practical solution.

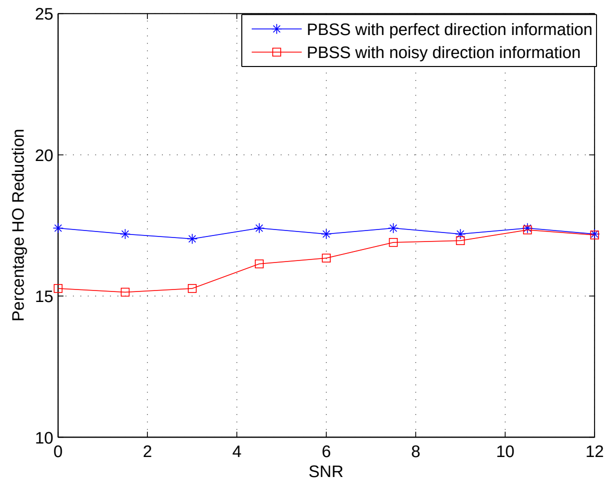

FIGURE 5.6. Performance of PBSS under non-ideal direction information.

In Fig. 5.6, the case where accurate direction information is not available is considered. The noisy direction information is defined as $d'_x = d_x + 1/\sqrt{\text{SNR}}\,\omega_x$ and $d'_y = d_y + 1/\sqrt{\text{SNR}}\,\omega_y$, where ω_x and ω_x are zero-mean normal random variables with unit variance. A simple detection mechanism is employed to obtain the estimates $\tilde{d}_x$ and $\tilde{d}_y$: $\tilde{d}_x = -1$, if d'_x is less than -0.33; $\tilde{d}_x = 0$, if $-0.33 \leq d'_x \leq 0.33$; and $\tilde{d}_x = 1$, otherwise. It is also assumed that $P_{\text{dir}} = 0.08$ and the speed of each MS is different. Fig. 5.6 shows that even if the direction data is not accurate, the proposed PBSS algorithm results in significant reduction in handover probability compared to the CBSS algorithm. PBSS algorithm compares the expected signal level of the MS to the serving/anchor BS with T_2, and in case this signal level is expected to be less than T_2, the handover is not executed and the same comparison is performed for the BS that has the next highest decision metric and so on.

To be able to numerically calculate the outage probabilities for PBSS and CBSS, $P_{PBSS}(r)$ and $P_{CBSS}(r)$ needs to be obtained. These probability density functions are depicted in Fig. 5.7, where it can bee seen that PBSS has a slightly higher mean and standard deviation.

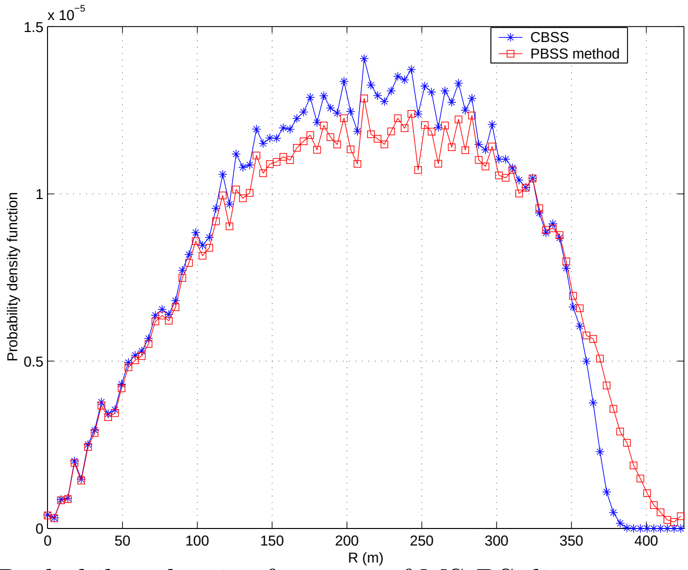

FIGURE 5.7. Probability density function of MS-BS distance with respect to the radius r for PBSS and CBSS.

By making use of Eq. 5.14, and numerically calculated $P_{PBSS}(r)$ and $P_{CBSS}(r)$ functions, the outage probability for CBSS and PBSS schemes are obtained to be 0.0115 and 0.0140, respectively. For these calculations, we have used the $\boldsymbol{P}_{\text{th}}$ value, calculated using Eq. 2.3 at the cell boundary. As shown by the results provided in this section, while PBSS decreases the number of handovers and therefore enhances the overall system performance, its outage probability is almost the same as CBSS.

5.5. Conclusion

In this chapter, a new handover decision algorithm for broadband wireless access systems called predictive base station switching is introduced. PBSS makes use of the mobile speed and direction information to calculate a specific decision metric for each neighboring/diversity-list base station, which is the ratio of the expected time period that the mobile station will be connected to a certain base station, and the average mobile-base distance while it is connected to a certain base station. A low-complexity method to calculate the mobile-base distance is also provided. It is demonstrated via simulation that even when the mobile station is expected to change direction in one out of every five time instants on the average, the handover reduction provided by the proposed PBSS is more than 17% and the degradation in the average signal level is within about half a dB compared with the existing signal-level based algorithms. Furthermore, even when the direction estimate of the mobile station is noisy, PBSS still performs considerably better than classical algorithms that are based only on signal level and BS-MS distance information. It is also shown that both methods have comparable outage probabilities.

6. CONCLUSIONS

6.1. Summary

Emerging wireless systems generally require more bandwidth, and higher data rates to address the requirements of the users. This fact results in the application of more sophisticated wireless communication schemes. Addressing the problems of these schemes, and improving their overall performance is thus a vital issue, and this thesis focuses on this fact.

The work in Chapter 3 focusses on the issue of estimating the maximum doppler frequency for OFDM systems, and thus for wireless systems (mainly WAN or WLAN) that utilize OFDM. In this chapter, a ML based algorithm is derived to estimate the maximum Doppler frequency in fast time-varying Rayleigh fading channels. To better estimate the maximum Doppler frequency, ICI, which occurs especially for fast time-varying is also modeled. This novel algorithm requires no extra overhead, as inherent pilot subcarriers are used for the process. With the complexity of the algorithm in mind, this approach allows certain coefficients of the system to be effectively be stored in the system memory. Another main advantage of the algorithm is that, for a majority of the cases, the delay profile information is not required to be known at the receiver side. Via many design parameters, it also possible to tailor this approach to fit the design requirements of a given system employing this approach. The Cramér-Rao bound for the MSE of the Doppler estimates are also provided, and simulation results verified the accuracy of the proposed algorithm.

Chapter 4 also focuses on wireless systems that employ OFDM systems. The purpose of the work presented in this chapter is to suppress the phase noise introduced by the local oscillator, which can cause significant performance degradation due to ICI it creates. The algorithm is designed specifically for doubly-selective channels, particularly those with a high normalized maximum Doppler frequency. A quasi-static fading model is unacceptable for this kind of channel models and thus a simple common phase error (CPE) term does not exist. This method is applicable to both phase-locked and free-running local oscillators. The algorithm is a maximum likelihood approach that exploits the pilot subcarriers as in Chapter 3, whose coefficients can be stored in the system memory to reduce the complexity.

In Chapter 5, a new handover decision algorithm for broadband wireless access systems called is introduced especially for emerging WAN systems. The proposed algorithm, predictive base station switching (PBSS), uses mobile speed and direction information to calculate a specific decision metric for each neighboring/diversity-list base station, which is later used to decide on the most appropriate handover strategy. The decision metric is the ratio of the expected time period that the mobile station will be connected to a certain base station, and the average mobile-base distance while it is connected to a certain base station. Furthermore, a low-complexity method to calculate the mobile-base distance is also provided. It is demonstrated with simulation results that even when the mobile station changes its direction frequently, the handover reduction provided by the proposed PBSS is very significant. Additionally, even when the direction information is not accurate, PBSS still performs considerably better than a classical algorithm. It is also shown that the two schemes have comparable outage probabilities.

6.2. Future Research

6.2.1. Future Research for ML Maximum Doppler Frequency Estimation

OFDM systems are specifically designed with a single user in mind. The multiple access scheme of OFDM, that allows simultaneous use of the channel by more than one user is called Orthogonal Frequency Division Multiple Access (OFDMA). Thus, a natural extension of the work presented in Chapter 3 is to apply this algorithm to OFDMA based systems.

6.2.2. Future Research for ML Phase Noise Suppression

Multiple-input multiple-output (MIMO), is the name of the scheme that allows the use of multiple antennae both at the transmitter and the receiver to increase the throughput by exploiting the space domain as these multiple antennae are considered to be physically separated in space. As the use of MIMO schemes in flat fading channels requires less complexity on the receiver side, and hence less power consumption, MIMO schemes are compatible with low-cost OFDM systems. Hence, future work of Chapter 4 should focus on applying the proposed algorithm to MIMO-OFDM systems.

BIBLIOGRAPHY

[1] Wi-Fi Alliance, "Enabling the Future of Wi-Fi Public Access" [online], Feb. 2004, available from World Wide Web: http://www.wi-fi.org/files/uploaded_files/wp_2_Future%20of%20Wi-Fi%20Public%20Access_1-2-04.pdf.

[2] J. Gao, O. C. Ozdural, S. H. Ardalan, and H. Liu, "Performance Modeling of MIMO OFDM Systems via Channel Analysis," *IEEE Trans. on Wireless Communications*, vol. 5, pp. 2358-2362, Sept. 2006.

[3] Wikipedia, "IEEE 802.11" [online], available from World Wide Web: http://en.wikipedia.org/wiki/IEEE_802.11.

[4] A. Bittau, M. Handley, J. Lackey,"The final nail in WEP's coffin," in *2006 IEEE Symposium on Security and Privacy*, May 2006.

[5] Bluetooth SIG, Bluetooth Specification Version 1.1, [online], available from World Wide Web: http://www.bluetooth.com.

[6] W. D. Jones, "No strings attached [wireless USB]," *IEEE Spectrum*, vol. 43, pp. 16-18, April 2006.

[7] Wikipedia, "Comparison of wireless data standards" [online], available from World Wide Web: http://en.wikipedia.org/wiki/Comparison_of_wireless_data_standards.

[8] A. Goldsmith, *Wireless Communications.* Cambridge University Press, 2005.

[9] *Supplement to IEEE Standard for Information TechnologyTelecommunications and Information Exchange Between SystemsLocal and Metropolitan Area NetworksSpecific Requirements. Part 11: Wireless Lan Medium Access Control (MAC) and Physical Layer (PHY)*, IEEE Standard 802.11a, Dec. 1999.

[10] *IEEE Standard for Local and Metropolitan Area Networks. Part 16: Air Interface for Fixed and Mobile Broadband Wireless Access Systems*, *IEEE Standard 802.16e*, Feb. 2006.

[11] P. A. Bello, "Selective fading limitations of the KATHRYN modem and some system design considerations," *IEEE Trans. on Commun. Technol.*, vol. 13, pp. 320-333, Sept. 1965.

[12] M. S. Zimmermann, and A. L. Kirsch, "The AN/GSC-10/KATHRYN variable rate data modem for HF radio," *IEEE Trans. on Commun. Technol.*, vol. 15, pp. 197-205, Apr. 1967.

[13] H. Liu and G. Li, *OFDM-Based Broadband Wireless Networks Design and Optimization*. John Wiley & Sons, 2005.

[14] A. R. S. Bahai and B. R. Saltzberg, *Multi-Carrier Digital Communications: Theory and Applications of OFDM*. Kluwer Academic Publishers, 2002.

[15] J. G. Proakis, *Digital Communications, Fourth Edition*. McGraw-Hill, 2001.

[16] H. Schulze and C. Lüders, *Theory and Applications of OFDM and CDMA Wideband Wireless Communications*. John Wiley & Sons, 2005.

[17] T. S. Rappaport, *Wireless Communications: Principles and Practice, Second Edition*. Prentice Hall PTR, 2002.

[18] J. M. Holtzman and A. Sampath, "Adaptive averaging methodology for handoffs in cellular systems," *IEEE Trans. on Vehicular Technology*, vol. 44, no. 1, pp. 59–66, Feb. 1995.

[19] L. Lindbom, "Adaptive equalization for fading mobile radio channels," *Licentiate Dissertation, Technology Dept., Uppsala Univ.*, Uppsala, Sweden, 1992.

[20] M. D. Austin and G. L. Stuber, "Eigen-based Doppler estimation for differentially coherent CPM," *IEEE Trans. on Vehicular Technology*, vol. 43, pp. 781–785, Mar. 1994.

[21] J. Cai, W. Song, and Z. Li, "Doppler spread estimation for mobile OFDM systems in Rayleigh fading channels," *IEEE Trans. on Consumer Electronics*, vol. 49, pp. 973–977, Nov. 2003.

[22] L. Krasny, H. Arslan, D. Koilpillai, and S. Chennakeshu, "Doppler spread estimation in mobile radio systems," *IEEE Communication Letters*, vol. 5, no. 5, pp. 197–199, May 2001.

[23] T. Yucek, R. M. A. Tannious, and H. Arslan, "Doppler spread estimation for wireless OFDM systems," in *2005 IEEE/Sarnoff Symposium on Advances in Wired and Wireless Communication*, pp. 233–236, Apr. 2005.

[24] Y.-S. Choi, P. J. Voltz, and F. A. Cassara, "On channel estimation and detection for multicarrier signals in fast and selective Rayleigh fading channels," *IEEE Trans. on Communications*, vol. 49, pp. 1375–1387, Aug. 2001.

[25] P. Stoica and R. Moses, *Introduction to Spectral Analysis*. Upper Saddle River, NJ:Prentice-Hall, 1997.

[26] T. Pollet, M. Van Bladel, and M. Moeneclaey, "BER sensitivity of OFDM systems to carrier frequency offset and Wiener phase noise," *IEEE Trans. Commun.*, vol. 43, no. 2/3/4, pp. 191-193, Feb./Mar./Apr. 1995.

[27] H. Li and H.-M. Rein, "Millimeter-wave VCOs with wide tuning range and low phase noise, fully integrated in a SiGe bipolar production technology," *IEEE J. Solid-State Circuits*, vol. 38, pp. 184–191, Feb. 2003.

[28] L. Piazzo, and P. Mandarini, "Analysis of phase noise effects in OFDM modems," *IEEE Trans. Commun.*, vol. 50, no. 10, pp. 1696–1705, Oct. 2002.

[29] P. Robertson, and S. Kaiser, "Analysis of the effects of phase noise in orthogonal frequency division multiplex systems," in *Proc. IEEE Int. Conf. Commun. (ICC'95)*, Seattle, WA, Jun. 1995, pp. 1652–1657.

[30] L. Tomba, "On the effect of Wiener phase noise in OFDM systems," *IEEE Trans. Commun.*, vol. 46, no. 5, pp. 580–583, May 1998.

[31] A. G. Armada, and M. Calvo, "Phase noise and sub-carrier spacing effects on the performance of an OFDM communication system," *IEEE Commun. Lett.*, vol. 2, no. 1, pp. 11–13, Jan. 1998.

[32] A. G. Armada, "Understanding the effects of phase noise in orthogonal frequency division multiplexing (OFDM)," *IEEE Trans. Broadcasting*, vol. 47, no. 2, pp. 153–159, Jun. 2001.

[33] P. Liu, S. Wu, and Y. Bar-Ness, "A phase noise mitigation scheme for MIMO WLANs with spatially correlated and imperfectly estimated channels," *IEEE Commun. Lett.*, vol. 10, no. 3, pp. 141–143, Mar. 2006.

[34] E. Panayirci, H. A. Cirpan, M. Moeneclaey and N. Noels, "Blind data detection in the presence of PLL Phase Noise by sequential Monte Carlo method," in *Proc. IEEE ICC'06*, Istanbul, Turkey, June 2006.

[35] W. C. Jakes, *Microwave Mobile Communications*. New York: Wiley, 1974.

[36] F. Munier, T. Eriksson and A. Svensson, "Receiver algorithms for OFDM systems in phase noise and AWGN," in *15th IEEE PIMRC'04*, Barcelona, Spain, Sept. 2004.

[37] A. Papoulis and S. U. Pillai, *Probability, Random Variables, and Stochastic Processes*. New York: McGraw-Hill, 2002.

[38] S. Wu, and Y. Bar-Ness, "A phase noise suppression algorithm for OFDM-based WLANs," *IEEE Commun. Lett.*, vol. 6, no. 12, pp. 535–537, Dec. 2002.

[39] S. Choi, G.-H Hwang, T. Kwon, A.-R. Lim and D.-H. Cho, "Fast handover scheme for real-time downlink services in IEEE 802.16e BWA system," *Proc. IEEE VTC'05-Spring*, Stockholm, Sweden, May-June 2005.

[40] J. M. Holtzman and A. Sampath, "Adaptive averaging methodology for handoffs in cellular systems," *IEEE Trans. Vehicular Technol.*, vol. 44, pp. 59-66, Feb. 1995.

[41] M. D. Austin and G. L. Stuber, "Velocity adaptive handoff algorithms for microcellular systems," *IEEE Trans. Vehicular Technol.*, vol. 43, pp. 549-561, Aug. 1994.

[42] R.-T. Juang, H.-P. Lin, D.-B. Lin and W.-C. Zeng, "Verification of mobility-based soft handover algorithm using WCDMA measurements data," in *Proc. IEEE VTC'06-Spring*, Melbourne, Australia, May 2006.

[43] M. D. Austin and G. L. Stuber, "Direction biased handoff algorithms for urban microcells," in *Proc. IEEE VTC'94*, Stockholm, Sweden, June 1994.

[44] R. Hsieh, Z. G. Zhou and A. Seneviratne, "S-MIP: a seamless handoff architecture for mobile IP," in *INFOCOM 2003*, San Franciso, CA, USA, Mar-Apr. 2003.

[45] Y.-S. Choi, O. C. Ozdural, H. Liu and S. Alamouti, "Maximum Likelihood Doppler Frequency Estimator for OFDM Systems," in *Proc. IEEE ICC'06*, Istanbul, Turkey, June 2006.

[46] M. A. Spirito, "On the accuracy of cellular mobile station location estimation," *IEEE Trans. Vehicular Technol.*, vol. 50, pp. 3674–685, May 2001.

[47] M. Aso, T. Saikawa and T. Hattori, "Mobile station location estimation using the maximum likelihood method in sector cell systems, in *Proc. IEEE VTC'02*, Vancouver, Canada, Sep. 2002.

[48] S. Ahonen and H. Laitinen, "Database correlation method for UMTS location," in *Proc. IEEE VTC'03-Spring*, Jeju , Korea, Apr. 2003.